AN ABSTRACT OF THE THESIS OF

Molly Glass for the degree of Master of Science in Nuclear Engineering presented on March 20, 2017.

Title: Effect of Initial Conditions and Depressurization on Lock Exchange Flow After a Depressurized Conduction Cool-Down Event in the High Temperature Test Facility

Abstract approved:

_____

Brian G. Woods

The High Temperature Test Facility (HTTF) is an electrically heated, scaled model of a Modular High Temperature Gas Reactor (MHTGR). Five experiments were conducted to study Depressurized Conduction Cool-Down phenomena stemming from a Double-Ended Guillotine Break (DEGB). After a DEGB, the reactor pressure vessel would depressurize until the pressures are equalized between the cavity that surrounds the reactor vessel and the vessel itself. Immediately following the depressurization there would be a large density gradient between the reactor vessel, which is full of hot helium and the cavity mixture of cold air and discharged helium. This density gradient would drive lock exchange flow, where the less dense helium would travel along the top of the pipe and the denser cavity gas would intrude into the bottom of the pipe and propagate towards the lower plenum. The cavity gas would then fill the lower plenum up to the top elevation of the hot leg pipe, which would then diffuse air into the core, potentially compromising core support and fuel integrity by graphite oxidation. Lock exchange flow is a density driven mechanism that

depends on the density gradient between the cavity and the pressure vessel. Gas concentrations and temperatures greatly affect density and thus affect key time characteristics of lock exchange flow. The key time characteristics to be studied in the five experiments are: the time for the gas front to arrive at the thermocouple instrumentation in the cross-duct outside the lower plenum, the time to fill the lower plenum, and the times to reach instrumented posts in the lower plenum at various heights. The time to reach the plenum will indicate the speed at which the cold dense gas front is travelling. The time to fill the lower plenum is also the time of onset of molecular diffusion. The time the gas front reaches each instrumented post will display how the cold dense gas front propagates through the plenum. The first three of five tests were conducted at ambient temperatures with initially equalized pressures between the Reactor Cavity Simulation Tank (RCST) and the Primary Pressure Vessel (PPV). The next test was a heated depressurization, and the last test was a heated test with pressures initially equalized. These three categories of tests vary initial conditions that will change lock exchange flow time characteristics.

Effect of Initial Conditions and Depressurization on Lock Exchange Flow After a Depressurized Conduction Cool-Down Event in the High Temperature Test Facility

by
Molly Glass

A THESIS
submitted to
Oregon State University

in partial fulfillment of
the requirements for the
degree of
Master of Science

Presented March 20, 2017
Commencement June 2017

Master of Science thesis of Molly Glass presented on March 20, 2017

APPROVED:

Major Professor, representing Nuclear Engineering

Head of the School of Nuclear Science and Engineering

Dean of the Graduate School

I understand that my thesis will become part of the permanent collection of Oregon State University libraries. My signature below authorizes release of my thesis to any reader upon request.

Molly Glass, Author

ACKNOWLEDGEMENTS

I would like to thank my family, Robert Glass, Michelle Lax, Allison Glass and Hunter Glass, for always encouraging me in all my pursuits. They have always provided me a safety net to fall back on so that I can fearlessly pursue my dreams. Without them I would not be here. My family and my closest friends will always be my most valued possession.

I want to thank my boyfriend, Oliver Hudson. He has always provided me with the strength and motivation to keep moving forward. I really appreciate his loving support and kindness throughout our relationship. He has buoyed me through difficult days and helped me to step back to really enjoy the good days.

I also want to thank my dog Mozic. He has been here for me for every single one of my graduations starting from elementary school, and he has seen me safely through my Master's thesis. He has been the best companion I could ever ask for.

Thanks to all my colleagues at the HTTF. Your help has been invaluable and your friendship has brightened many cloudy Corvallis days. Special thanks to Matt Hertel, Dr. Cadell, and Dr. Gutowska for answering a seemingly ceaseless stream of questions.

I have so much appreciation for my advisor Dr. Brian Woods. I am not always the easiest student. I always push myself to do more and maintain perfection, and I am too stubborn to take no for an answer. And when I approached him to add a last-minute graduate certificate in Geographic Information Systems, he believed in me and my ambitious goals.

TABLE OF CONTENTS

Page

TABLE OF CONTENTS (Continued)

Page

LIST OF FIGURES

LIST OF FIGURES (Continued)

Figure Page

LIST OF FIGURES (Continued)

Figure Page

LIST OF FIGURES (Continued)

Figure Page

LIST OF TABLES

LIST OF ABBREVIATIONS

HTGR = High Temperature Gas Reactor

HTTF = High Temperature Test Facility

MHTGR = Modular High Temperature Gas Reactor

RPV = Reactor Pressure Vessel

D-LOFC = Depressurized Loss of Forced Convection

DCC = Depressurized Conduction Cool-Down

PIRT = Phenomena Identification and Ranking Table

RCST= Reactor Cavity Simulation Tank

OSU = Oregon State University

DEGB = Double-Ended Guillotine Break

LIST OF NOMENCATURE

κ_m = mass diffusion coefficient (assumed constant)

d_{Brk} = hot leg diameter

L_{Brk} = distance between break and entrance to the lower plenum

u_{Brk} = velocity of the hot Helium approaching the cold gas plume

τ = time constant

ρ^+ = normalized density with the initial density of the nitrogen in the cavity

t^+ = normalized time with the time constant

u_z^+ = normalized velocity of the jet along the length of the duct

z^+ = normalized length with the distance between break and lower plenum entrance

r^+ = normalized radius with the diameter of the break

θ^+ = normalized angle

μ^+ = normalized dynamic viscosity

P_0 = initial pressure (equal on either side of the break upon accident initiation)

g_z = gravity term in z

g_r = gravity term in r

g_θ = gravity term in θ

$\rho_{cavity,0}$ = density of the nitrogen from the cavity initially

P^+ = normalized pressure with initial pressure

$\mu_{cavity,0}$ = dynamic viscosity of the nitrogen from the cavity initially

1. Introduction

1.1 Background

A renewed interest in VHTRs emerged because of the Energy Policy Act of 2005. The intention of the policy was to determine the next generation nuclear plant. It is required that the reactor not only produce electricity but also hydrogen, and the intention was for a reactor to be operational by September 2021. In addition to these requirements, new reactor technology aims to have more accurate safety calculations to enable operation at higher powers. The current fleet of nuclear reactors operates well within safety margins that are known to be conservative, however have large uncertainty. By increasing the accuracy of safety calculations, uncertainty is reduced and operators can have more operating flexibility and potentially increase power output while staying within the current safety limits [1].

Safety margins are related to the limits of the reactor materials in accident scenarios. Maximum clad and fuel temperatures are a focus of safety studies. It is suspected that DCC and PCC events will be the most demanding on the reactor and the most likely to have maximum clad and fuel temperatures. Thus, the parameters that surround the DCC and PCC events bound the operating temperatures for the VHTR and must be fully understood for licensing purposes [1].

The VHTR has been defined as a reactor whose bulk outlet temperature is above 900°C. The high temperature ensures high reactor efficiency and high temperature process heat for other applications [1]. There are two main VHTR designs. One design is prismatic block, where TRISO fuel is compacted into multiple graphite blocks. These blocks are stacked together and have coolant and instrumentation channels inside the blocks. The second design is the pebble bed reactor. This reactor also uses TRISO fuel but instead of refueling with graphite blocks they utilize a constant movement of fuel pebbles inside the core, exchanging pebbles when needed, so the reactor does not need to go offline for refueling [1].

There are several strengths and weaknesses for each of the designs. The United States has more fabrication and operating experience with prismatic block designs. In addition, the position of coolant channels and the fuel is known and

controllable, thus peak fuel temperature is more predictable and control rod placement is easier. The weaknesses are that the prismatic design needs larger excess reactivity, higher control rod worth and high packing fractions for startup. Refueling is a long process and the fuel at the hot spot location remains there from startup until refueling. In addition, if there was water ingress, there would be a relatively strong reactivity increase [1].

The strength of the pebble bed is that the fuel is utilized well because burnup is more even for each fuel pebble as a result of its movement and little excess reactivity is needed for startup. Water ingress and reactivity insertion are not major safety concerns because of the smaller excess reactivity. Pebble beds also do not require refueling outages and fuel enrichment is lower, thus peak temperature in fuel will probably be lower. However, it is more difficult to calculate flow and temperature variations because the pebbles are constantly moving and exact positions cannot be known. The pebbles create a large pressure drop across the core and there is the potential that a fuel pebble could get stuck in the recycling mechanism that shuffles the fuel from the bottom of the core to the top or the pneumatic tubes that can insert fresh fuel pebbles. Creation of dust is also a concern. Licensing the pebble bed design could be more difficult because moving fuel increases uncertainty in multiple types of calculations [1].

The energy policy calls for the production of electricity as well as hydrogen to potentially power transportation in the future [2]. Additionally, lowering carbon dioxide emissions is vital in response to climate change. As of 2007, only 20% of electrical power is supplied by nuclear and 50% by coal [1]. High Temperature Gas Reactors (HTGRs) can contribute to economies aside from electricity production; they can cogenerate electricity and steam for residential and commercial building heating and produce process heat for industrial applications like coal gasification and desalination. No additional costs exist other than running the plant for electricity generation to produce the secondary benefits of steam and process heat for additional energy consumption needs [1], [2].

Although VHTR and MHTGR (Modular High Temperature Gas Reactor) are used interchangeably for the purposes of this document, the VHTR operates at higher

temperatures to increase efficiency. The MHTGR is a prismatic block reactor designed by General Atomics. It operates at 6.4 MPa and an inlet temperature of 259ºC and an outlet temperature of 687ºC. It utilizes helium as a coolant and has a modular design so that pieces of the reactor can be fabricated offsite to reduce capital costs [3]. MHTGRs have a higher thermal efficiency, passive safety features, easy refueling, advantageous fuel integrity and proliferation resistance compared to light water reactors, and are ideal for remote areas [4]–[6]. They can use different types of fuel, including plutonium-239, and high and low enriched uranium and its fuel retains radionuclides better for long term disposal [7]. However, HTGR deployment has many obstacles, including an expectation of "catastrophe free" nuclear power, which ensures that radioactive substances are always contained on site even in the event of an accident [8].

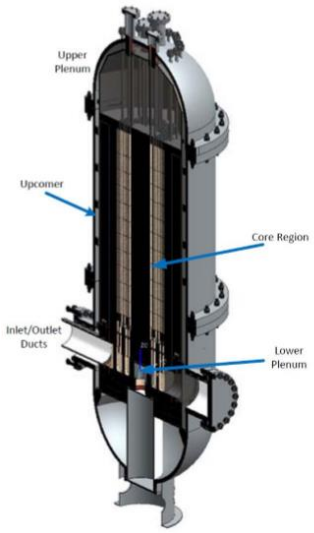

Figure 1: The HTTF Primary Pressure Vessel Design [9].

The High Temperature Test Facility (HTTF) is a scaled, electric model at Oregon State University (OSU) of the MHTGR as shown in Figure 1 [3]. There are a few major differences between the prototype and the OSU facility. The MHTGR sits inside a cavity filled with air. In the HTTF the primary pressure vessel (PPV) and the reactor cavity simulation tank (RCST) are in two separate tanks connected by a crossover duct. The RCST in the HTTF is also filled with nitrogen instead of air. The crossover duct in the HTTF is similar to the crossover duct that would be seen between the reactor core and the steam generator in the MHTGR. The separation of

the two tanks allows for the facility to open two main break valves simulating a Double-Ended Guillotine Break (DEGB) of the cross over duct. This break would cause a depressurization of the reactor and a loss of flow. It is called the Depressurized Loss of Forced Convection Accident (D-LOFC), also known as the Depressurized Conduction Cool-Down (DCC) Event for HTGRs because heat removal is by conduction through the core and radiation out of the vessel [9].

A DCC event assumes 100% power at the onset of the accident. The hot and cold legs are then both broken and the reactor blows down quickly. The reactor trips to power down and heat production is reduced to decay heat level, however, the core continues to heat because of the loss of forced convection. The power conversion unit is disconnected and thus does not play a large part of the accident progression. Helium discharge purges some air from the cavity but also releases graphite dust into the cavity. The discharge is filtered through vents to reduce the environmental impact of the radioactive dust. Once depressurization has finished, air enters the vessel by lock exchange flow as shown in Figure 2 below. The more dense air travels along the bottom of the hot duct to fill the lower plenum up to the top elevation of the hot leg.

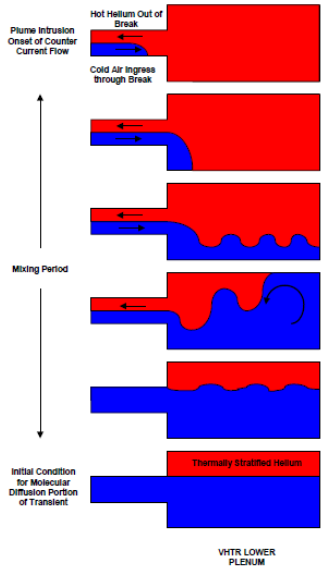

Figure 2: Progression of the lock exchange flow in the hot leg after a DCC event

If the graphite has a high enough temperature a chemical oxidation reaction could occur between the graphite and the air. This reaction could compromise the integrity of the core structural support in the lower plenum as well as the reactor core

itself after the onset of natural circulation. It is suggested in research that the longer it takes for air ingress to start, the more time the lower plenum has to cool and thus less oxidation would occur there. However, the core would still be hot, so the oxidation could occur in the core instead of the lower plenum [10]. Oxidation in the lower plenum may reduce the oxygen concentrations that will reach the core, but could accelerate the time to onset of natural circulation through the generation of carbon monoxide that will travel to the top of the reactor vessel displacing helium and entraining air in the process [1], [4]. Certain models have also indicated that oxidation may increase with the additional heat generated from the oxidation itself [11]. Graphite oxidation could generate a large amount of heat, exacerbating peak vessel wall or fuel temperatures [1]. Once there is no forced convection cooling, heat removal is driven by the RCCS as the core conducts heat outward and then radiates the heat from the vessel wall to the RCCS.

1.2 Objective

1.2.1 Purpose

The purpose of this experiment is to evaluate the impact of initial pressures in the HTTF vessel and cavity on the progress of lock exchange flow through the crossover ducts and in the lower plenum. The driving mechanism of lock exchange flow is the density gradient between the vessel and the cavity. The differences in density and buoyancy of the constituents will create two layers inside the duct with the progression scheme as shown in the figure 2. The initial conditions of lock exchange flow are highly dependent on depressurization, which could change gas compositions and temperature distributions in the vessel and the cavity.

First, HTTF scaling and distortion and previous studies on lock exchange flow will be explored. Then, the experiments will use thermocouples in the RCST, crossover duct and lower plenum to evaluate key time characteristics of lock exchange flow for pressure equalized ambient tests, a pressure equalized heated test as well as a heated depressurization test. The time characteristics that will be explored are the arrival of the gas front at instrumented locations in the duct, the arrival of the gas front at the lower plenum instrumented posts, and the time to fill up the lower plenum with a nitrogen gas layer. The time to stratify the lower plenum to

the top of the elevation of the hot duct is a quasi-equilibrium state for molecular diffusion to commence between the thermally stratified helium and the cavity gas layers [12]. It does not consider the potential effects of the nitrogen thermally expanding up into the core as it is heated. The time characteristics will be compared between the experiments.

Examination of the lower plenum thermocouples will show the times of arrival of the nitrogen gas front and how the gas front propagates through the lower plenum. The plenum posts are instrumented at various heights to allow examination of the filling of the lower plenum [13].

1.2.2 Experiment

The HTTF will be conducting lock exchange flow scenarios with various initial conditions. This study will analyze the lock exchange flow and lower plenum fill up after opening the double guillotine valves to compare phenomena that occur after a DCC event. Thermocouples will be used to characterize the gases inside the duct, the lower plenum, and the RCST.

1.2.3 Figures of Merit

To meet the purpose of the experiment, certain data must be gathered and analyzed with a high confidence in the fidelity of the test. To ensure success of the experiments, the following goals have been set to be observable:

1. Time to fill the lower plenum, which will indicate the onset of molecular diffusion between the thermally stratified helium and cavity gas layer.
2. Time for helium front to reach the instrumentation in the duct in the RCST and the time for the nitrogen front to reach the instrumentation in the duct 8.5 inches from the PPV outlet.
3. Time of arrival at instrumented lower plenum posts, which will display the gas propagation scheme in the lower plenum.

1.3 Limitations

2. The HTTF is scaled to one eighth of the pressure at .8 MPa, therefore, data on the full depressurization will not be available. Focus will be limited to depressurization of .8 MPa at most. The depressurization still experiences choked flow and pre-test calculations indicate that a full depressurization

would not significantly affect the results [14]. The RCST is limited to a pressure of 153 kPa gauge.

3. The experiment will be conducted on a non-prototypical design (HTTF) for the MHTGR. Of the main parameters, the height and diameter are one fourth the size of General Atomics' prototype. The pressure is one eighth scale. The temperature remains prototypical. The core is ceramic instead of graphite so that temperature profiles can be maintained for a smaller volume. Scaling has been assessed so that results can be translated to a full-scale model.
4. The duct break can only be conducted at one location in the duct.
5. The RCST will be filled with nitrogen instead of air. In the prototype, the cavity surrounding the MHTGR is air, however, the HTTF uses nitrogen instead because the graphite heater rods are susceptible to oxidation [15].
6. The cross over duct break consists of opening valves for the hot and the cold legs which are concentric pipes at the entrance to the PPV. The cold leg is separated from the hot leg to enter the RCST as a separate pipe with a separate break valve.
7. The valve on the hot leg has a 14 second actuation time. The valve on the cold leg has a 10 second actuation time. The valves are not opened simultaneously; there is a several second gap in opening the valves.
8. The facility's bottom core block protrudes down further than the top height of the hot duct entrance. This will introduce additional form loss for the filling of the lower plenum. The change from the prototype to the facility was created by scaling the vessel height by one fourth and the hot duct entrance diameter by one fourth.

1.4 Assumptions

1. Opening a valve is equal to a double ended guillotine break. It is assumed that the no slip condition on the valve does not impact the results in addition to the extended actuation time.
2. The instrumentation inside the facility does not significantly affect the results.
3. Graphite oxidation would not affect lock exchange flow
4. The gas that is already present in the steam generator will prevent gas from

travelling up through the steam generator during the transient accident

1.5 Motivation

There is a very limited amount of research available on the depressurization phase of the DCC event and how it will affect the subsequent phases. Momentum driven depressurizing flow may delay lock exchange flow and consequently the onset of natural circulation [14]. The vital concern is the rate and concentration of air ingress that is dependent on initial boundary conditions.

Only recently has lock exchange flow been considered during a DCC event. Before, the process was depressurization, molecular diffusion, and then natural circulation [16], [17] and experimental results in vertical channels like Germany's NACOK and Japan's HTTR research reactors supported the hypothesis that molecular diffusion was the driving force for air ingress [17], [18], but now it is known that a very large part of air ingress is lock exchange flow. The GTMHR design uses a horizontal cross duct and more tests need to be conducted to fully understand lock exchange flow and how it affects air ingress during a DCC [1].

Understanding the behavior of the reactor during a DCC event is of the highest priority for research and development for the VHTR [1]. Codes are being created to best simulate the flow so that the proper correlations can be developed for the use of one-dimensional system codes, however the results must be validated with experimental data [1]. Light water reactor software tools have been extensively tested and vetted for safety analyses, but high temperature gas reactors need their own tools which need to be verified and validated with experimental data to the satisfaction of the Nuclear Regulatory Commission, thus instilling a confidence in modeling phenomena with proven accuracy and fidelity [1], [5].

It was emphasized by the Nuclear Regulatory Commission in the Phenomena Identification Ranking Tables (PIRTs) that more knowledge regarding the rate and concentration of air ingress during a DCC is required because of the potential oxidation consequences of the graphite structure support and core [5], [19]. A DEGB of the crossover duct is extremely unlikely, however due to the high potential consequences, it is necessary to certify that the safety of the reactor is maintained during a DCC air ingress event [19].

1.6 Outline

Chapter 2 covers the literature review. It includes the scaling and distortion between the HTTF and the MHTGR. The general progression of the DCC event is then reviewed, detailing depressurization and lock exchange flow, highlighting the differences between molecular diffusion studies and stratified flow for driving mechanisms of air ingress. Previous work in lock exchange flow and lower plenum flow is reviewed.

Chapter 3 details the design of the HTTF, highlighting differences in the HTTF geometry with the prototypical geometry. It reviews the instrumentation and error in the facility.

Chapter 4 includes results from DCC 1, 2 and 3. Study of DCC 1, 2, and 3 is limited, however, because of the small temperature difference present in the tests. DCC 4 and DCC 5 are studied more in depth including lower plenum thermocouple analysis.

Chapter 5 comprises the discussion of results that address the figures of merit of the experiment. Conclusions and future work are then detailed.

Chapter 6 is the bibliography of references for this work.

Chapter 7 contains an appendix of instrumentation

2. Literature Review

2.1 Scaling and Distortion between the HTTF and the MHTGR

2.1.1 Scaling

To ensure proper scaling of the HTTF, the hierarchical two-tiered scaling method was used (H2TS). H2TS combines top-down and bottom-up scaling approaches to ensure the scaling is systematic, traceable, and that data is applicable to a full-scale model while concurrently calculating distortion [13], [20].

Top down scaling creates non-dimensional Pi groups in terms of time ratios between the prototype and the facility for phenomena. Top down subdivides the integral system into interacting subsystems, then each subsystem into modules, each module into constituents and each constituent into phases. For each of the constituents there is a geometrical configuration that have three field equations: conservation of mass, momentum and energy. Each of these fields can be characterized by several processes, in this case, air ingress [20]. Top down scaling was used to identify important processes to be analyzed with bottom up scaling.

Bottom up scaling identifies the phenomena that the facility wants to model with the most fidelity to determine which similarity ratios are the most important and where distortion is acceptable. Then applicability of experimental data for a full-scale system is demonstrated using nondimensionalization, codes and simulation [12].

The HTTF was built to most accurately model the DCC event [1]. For an air ingress event, air concentration throughout the model must be comparable to the prototype during a DCC. The scaling report documents a set of similarity criteria; from these, kinematic similarity and friction and form loss similarity were determined to be paramount to scaling a DCC event [12]. The main non-dimensional scaling equations for conservation of mass, momentum and energy for a DCC exchange flow are as follows:

$$\frac{L_{Brk}}{\pi u_{Brk}}\frac{\partial \rho^{+}}{\partial t^{+}}+\frac{\partial}{\partial z^{+}}(\rho^{+}u_{z}^{+})=\frac{\kappa_{m}}{u_{Brk}d_{Brk}}\times\left[\frac{L_{Brk}}{d_{Brk}}\frac{1}{r^{+}}\frac{\partial}{\partial r^{+}}(r^{+}\frac{\partial \rho^{+}}{\partial r^{+}})+\frac{L_{Brk}}{d_{Brk}}\frac{1}{r^{+}r^{+}}\frac{\partial^{2}\rho^{+}}{\partial \theta^{+}\theta^{+}}+\frac{d_{Brk}}{L_{Brk}}\frac{\partial^{2}\rho^{+}}{\partial z^{+}\partial z^{+}}\right]. \quad (1)$$

$$\frac{L_{Brk}}{\pi u_{Brk}}\rho^{+}\frac{\partial u_z^{+}}{\partial t^{+}}+\rho^{+}u_z^{+}\frac{\partial u_z^{+}}{\partial z^{+}}=-\frac{P_0}{\rho_{cavity,0}u_{Brk}^2}\left(-\frac{\partial P^{+}}{\partial z^{+}}\right)+$$
$$\frac{\mu_{cavity,0}}{\rho_{cavity,0}u_{Brk}d_{Brk}}\left[\left(\frac{d_{Brk}}{L_{Brk}}\right)\frac{\partial}{\partial z^{+}}\left(\frac{4}{3}\mu^{+}\frac{\partial u_z^{+}}{\partial z^{+}}\right)+\left(\frac{L_{Brk}}{d_{Brk}}\right)\frac{1}{r^{+}}\frac{\partial}{\partial r^{+}}\left(\mu^{+}r^{+}\frac{\partial u_z^{+}}{\partial r^{+}}\right)+\left(\frac{L_{Brk}}{d_{Brk}}\right)\frac{1}{r^{+}}\frac{\partial}{\partial\theta^{+}}\left(\frac{\mu^{+}}{r^{+}}\frac{\partial u_z^{+}}{\partial\theta^{+}}\right)\right]+$$
$$\frac{g_z L_{Brk}}{u_{Brk}^2}\rho^{+}. \tag{2}$$

$$0=-\frac{\partial P^{+}}{\partial r^{+}}+\frac{\mu_{cavity,0}u_{Brk}}{P_0 L_{Brk}}\times\left[\frac{1}{r^{+}}\frac{\partial}{\partial r^{+}}(-\frac{2}{3}\mu^{+}r^{+}\frac{\partial u_z^{+}}{\partial z^{+}})+\frac{\partial}{\partial z^{+}}\left(\mu^{+}\frac{\partial u_z^{+}}{\partial r^{+}}\right)+\frac{2}{3}\frac{\mu^{+}}{r^{+}}\frac{\partial u_z^{+}}{\partial z^{+}}\right]+\frac{\rho_{cavity,0}g_r d_{Brk}}{P_0}\rho^{+}. \tag{3}$$

$$0=-\frac{1}{r^{+}}\frac{\partial P^{+}}{\partial\theta^{+}}+\frac{\mu_{cavity,0}u_{Brk}}{P_0 L_{Brk}}\times\left[\frac{1}{r^{+}}\frac{\partial}{\partial\theta^{+}}(-\frac{2}{3}\mu^{+}\frac{\partial u_z^{+}}{\partial z^{+}})+\frac{\partial}{\partial z^{+}}\left(\frac{\mu^{+}}{r^{+}}\frac{\partial u_z^{+}}{\partial\theta^{+}}\right)\right]+\frac{\rho_{cavity,0}g_r d_{Brk}}{P_0}\rho^{+}. \tag{4}$$

These equations are applicable for any non-dimensional buoyant jet in any break orientation when the velocity along the axis is greater than the velocity across or around the axis. The scaling report contains the full scaling analogies between the HTTF and the MHTGR [12].

2.1.2 Important Parameters

Important parameters between the HTTF and the MHTGR are then determined by the scaling equations. The Pi groups were analyzed by Woods et al. for distortions between the MHTGR and the HTTF as shown in Table 1 below [12].

Characteristic Ratio	Equation	Ratio (HTTF/MHTGR)	Distortion
$(\Pi_{G,EF})_R$	$\left(\frac{d_{Brk}}{L_{Brk}}\right)_R$	Varies (<1:4.1)	>0.76
$(\Pi_{\Delta\rho,EF})_R$	$\left(\frac{\rho_{cavity,0}-\rho_{vessel,0}}{\rho_{cavity,0}}\right)_R$	1:1 (concentration of Nitrogen and Helium in cavity gas can be adjusted to match ratios)	0.00
$(\Pi_{Pe,EF})_R$	$\left(\frac{u_{Brk}d_{Brk}}{\kappa_t}\right)_R$	1:1	0.00
$(\Pi_{Re,EF,H})_R$	$\left(\frac{\left[\rho_{cavity,0}\left(\rho_{cavity,0}-\rho_{vessel,0}\right)\right]^{1/2}d_{Brk}^{3/2}}{\mu_{cavity,0}}\right)_R$	1:6.5 (For density ratio = 1:1)	0.85
$(u_{Brk,EF,H})_R$	$\left(\frac{d_{Brk}\left(\rho_{cavity,0}-\rho_{vessel,0}\right)}{\rho_{cavity,0}}\right)_R^{1/2}$	1:1.9	—
$(t_{EF,H})_R$	$\left(\frac{\rho_{cavity,0}}{\rho_{cavity,0}-\rho_{vessel,0}}\right)_R^{1/2}\left(\frac{Ld^2}{d_{Brk}^{5/2}}\right)_R$	1:2.8	—

Table 1:Pi groups display distortion between HTTF [12].

2.2 General DCC Event, Depressurization and Lock Exchange Flow

In a MHTGR, the cavity surrounding the plant is filled with air and the cross duct connects the primary system to the secondary power conversion equipment. The reactor is running at 100% power when there is an instantaneous break of the crossover duct. This break does not affect any other core geometry [9].

2.2.1 Depressurization

The pressure operating condition for a MHTGR is at 6.4 MPa. The reactor pressure vessel will depressurize into the cavity surrounding the vessel. During depressurization, helium is released into the cavity via choked flow, if the pressure gradient between the upstream and downstream pressures is larger than 2.049 [15].

When the vessel depressurizes, a Reimann tube shock wave propagates outwards toward the lower density and compresses in the direction the wave is travelling. An expansion wave propagates in the opposite direction. The expansion wave will bounce off the walls of the lower plenum. Flow oscillations due to flow reversal and rarefication waves could influence the initiation and speed of air ingress by gas mixing which lowers the density gradient [15], [21].

The initial expansion causes the temperature of the core to decrease, however, the gas temperature recovers quickly, varying between 1 and 15 seconds depending on the heat transfer coefficient. In a median case of considering the heat transfer between the wall and the gas and the core materials and the gas as a median value, the heat transfer coefficient is $10 W/(m^2 K)$ and the recovery time is 3 seconds, which is on the same time scale as air ingress [16].

2.2.2 The Two Stages of Stratified Flow

After equal pressures are established, air will enter via stratified flow because of the density difference between the inside and the outside of the vessel, assuming no effect of momentum driven flow after depressurization. Outside of the vessel, the air-helium mixture has a significantly higher molecular weight and lower initial temperature compared to the helium in the reactor vessel.

The basic concept of lock exchange flow consists of two tanks of the same pressure that contain different density fluids connected by a horizontally oriented pipe with a barrier in the middle of the pipe to separate the tanks. When the barrier is

removed, the fluids will intrude into each other with the lesser density fluid travelling along the top of the pipe and the higher density fluid travelling along the bottom of the pipe in a stratified manner. The higher density fluid will fill up the bottom of the tank that once held only the lower density fluid. This process will continue until the bottom of the low-density tank is filled up to the top elevation of the broken pipe [22].

There are two stages of stratified flow. The first involves the density differences generated by different molecular masses as well as different temperatures between the inside and the outside of the reactor. The second depends on only the temperature difference between the inside and the outside changing their relative densities, which will continue until the onset of natural circulation and possibly afterwards [22].

The hot leg is a greater concern for air ingress than the cold leg because the air-helium mixture would have to travel up the upcomer to access the core from the cold leg. The hot leg provides direct access to the lower plenum and subsequently the core from the break. The air-helium mixture in the hot leg will start to pool at the bottom of the reactor vessel in the lower plenum. As the air heats, it will expand in addition to molecularly diffusing upwards into the core [1], [22].

2.2.3 Molecular Diffusion vs. Lock Exchange Flow

Before 2007, air ingress after a DCC event was characterized by 3 phases: depressurization, molecular diffusion, and natural circulation and the phases were corroborated with vertical chimney tests [17], [18]. Now it is known that lock exchange flow has a large impact on air ingress after a DCC for designs with horizontally oriented crossover ducts. Overall, natural circulation occurs much earlier than previous studies because lock exchange flow is much faster than molecular diffusion [22].

For other models to be comparable to that of the HTTF, the crossover duct must be horizontally oriented. In models that have a vertical crossover duct, like NACOK in Germany, density driven lock exchange flow may not be the driving mechanism of air ingress over molecular diffusion; experimentation supports the hypothesis that molecular diffusion is dominate in models with vertical chimneys like

the HTTR and NACOK because no local density gradient exists [11], [17], [18]. One way to determine the driving mechanism after a DEGB is to compare the pressure build-up and the hydrostatic head. Comparing the pressure build-up and hydrostatic head in the GT-MHR and the NACOK reveals that the pressure build-up in the GT-MHR is larger than the static head but the pressure build-up in the NACOK was much smaller than the static head. Therefore, the NACOK is dominated by molecular diffusion and the GT-MHR is dominated by the density gradient as shown in the table below [4].

Parameters	GTMHR	NACOK
Air Density Ratio (γ)	0.253	0.323
Pipe Diameter (D)	1.5 m	0.125 m
Core Height (Hv)	11 m	7.334 m
Pressure Build-up (dP)	24.18 Pa	1.101 Pa
Static Head	10.01 Pa	9.6 Pa

Table 2: The table compares the pressure build-up in the GTMHR to the NACOK facility [4].[1]

A Pi term was also created to compare pressure build-up vs. static head during stage two of air ingress, which physically means that if Π_2 is greater than 1 then the air will have enough buoyancy force to overcome the static head and start natural circulation, otherwise the stage is dominated by molecular diffusion[4], [22], [23]:

$$\frac{\Delta P}{Hydrostatic\ Head} > 1$$

$$\Pi_2 = \frac{1}{8}\left(\frac{H}{H_v}\right)\cdot\left(\frac{\rho_A}{\rho_{core}-\rho_{riser}}\right)\left(\frac{(1-\gamma)*(1-\gamma^3)}{\gamma^3}\right) > 1$$

$$H = diameter\ of\ horizontal\ pipe$$

$$H_v = height\ of\ the\ core$$ [4], [22], [23]

Another way to determine the driving mechanism is to examine the time scales of the density driven phenomena in NACOK vs. in the GTMHR [11].

2.2.4 Concerns over Mitigation Time Frame

The main concern for a density driven system rather than a molecularly driven system is the accelerated air ingress into the reactor. A shorter time of air ingress decreases the amount of time operators have to implement a mitigation strategy after an accident. Molecular diffusion air ingress studies found that time for the cavity gas

[1] "Reprinted from FY-09 Report: Experimental Validation of Stratified Flow Phenomena, Graphite Oxidation, and Mitigation Strategies of Air Ingress Accidents INL/EXT-09-16465, Rev. 1, Chang H. Oh, Eung S. Kim, Hyung S. Kang, Hee C. No, and Nam Z. Cho, page 2-27, December 2009, with permission from INL."

to reach the lower plenum was 150 hours [22]. Now, using lock exchange flow similar to theoretical models of Benjamin, time to arrival for cavity gas to enter the lower plenum is approximately 10 seconds [22], [24].

A faster air ingress event also creates a different set of boundary conditions for the onset of natural circulation than suggested in previous research which could accelerate oxidation inside the reactor. The reactor core would be at a higher temperature as the air ingresses, which could potentially release carbon monoxide with the oxidation reaction. Increasing temperatures in the core also increases the diffusivity of radioactive nuclides in the fuel, potentially creating a larger environmental impact. Thus, more studies in air ingress must be made to better understand this time sensitive phenomena with respect to adequate codes and validation with experimentation [22].

2.3 Previous work on Lock Exchange Flow

Lock exchange flow has been a subject of interest for many decades as it relates to multiple disciplines including toxic chemical releases, avalanches, and water intrusion into the ocean during dam breaks [24]. Lock exchange flow is also an inherent characteristic of passive systems used in advanced reactors [23]. However, there are some vital differences between the lock exchange flow tests that were conducted in other fields and the lock exchange flow that will occur after a DCC event in an MHTGR. This section will explore some of those differences and how it will change the flow.

2.3.1 Rectangular Channels

Many earlier tests used rectangular channels. In rectangular channels, the flow rates of the light and heavy fluids are identical [25], thus it was assumed the same condition applies to circular cross-section pipes. However, rectangular ducts have a constant current speed along the axis, which will maintain a constant flow regime and circular pipes have different depths as the fluid nears the sides of the pipe, which changes the speed and possibly the regime of the flow [22].

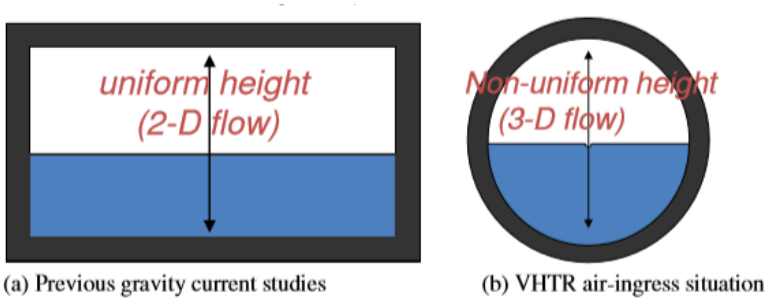

Figure 3: Shows how the shape of the duct may change the flow [4].[2]

With this fundamental difference, it was INL's goal to assess if rectangular models are still valid for cylindrical ducts. They built a scaled-down facility of General Atomics GTMHR crossover duct design with water and brine as the experiment fluids. INL reached Reynolds numbers between 2.34×10^4 and 3.79×10^5, which are similar to the postulated numbers of a DEGB accident. At these Reynolds numbers the flow is inviscid and frictional loss is negligible. The speed of the heavy current was found to be constant in the axial direction because the high Reynolds number, showing similar results to lock exchange flow in a rectangular duct as well as Benjamin's lock exchange flow theory [22], [24].

	Rectangular Pipe	**Circular Pipe**
Water	0.29 m/s	0.31 m/s
Brine	0.34 m/s	0.355 m/s

Table 3: Water and Brine Experiment Results for rectangular and circular pipes

The water and brine experiment results in Table 3 suggest that cylindrical geometry would contribute to a slightly faster air ingress rate than analytical models made for rectangular channels [4].

2.3.2 Boussinesq vs. non-Boussinesq flows

Additionally, most research was conducted on two fluids with low density differences, which categorizes the density driven flow in the Boussinesq regime. However, lock exchange flow for the HTGR will be in the non-Boussinesq regime. It was highlighted that tools need to be developed and verified for stratified flow behavior after the flow becomes unchoked from depressurization for densimetric

[2] "Reprinted from FY-09 Report: Experimental Validation of Stratified Flow Phenomena, Graphite Oxidation, and Mitigation Strategies of Air Ingress Accidents INL/EXT-09-16465, Rev. 1, Chang H. Oh, Eung S. Kim, Hyung S. Kang, Hee C. No, and Nam Z. Cho, page 3-3, December 2009, with permission from INL."

Froude numbers less than 1 in the NGNP Methods Technical Plan [1].

Benjamin wrote about gravity currents theoretically, balancing horizontal momentum with hydrostatic force. Without any losses, the gravity current would meet in the middle of the channel, with the lower half as the heavier gas and the upper half as the lighter gas. Lock exchange flows center around the idea that the heavier fluid has a larger piezometric pressure, thus displacing the lighter fluid to the top of the channel. The front moves with a constant speed and has a characteristic 'head wave' that comes up higher than the midway point and then dips down lower suggesting a turbulent zone behind the head wave [24], [26]. The speeds of the two wedges differ in proportion to the difference in their densities, however, not greatly [24].

Lowe, Rottman, and Linden (LRL) examined theory and experiments surrounding the non-Boussinesq lock-exchange problem. Their experiments were conducted with high Reynolds numbers based on the speed, depth and kinematic viscosity of the heavy current [27].

In the LRL experiments, it was noted that the heavier fluid front moved faster than the lighter fluid in a non-Boussinesq flow regime which contrasted with the Boussinesq flow of the same experiment where the velocities of the two fluids were approximately the same. The depth of the dense layer is less than that of the light fluid as the two layers cannot have the same depths and different speeds. The depths of the two layers must be different to conserve energy [27]. The volume flux of the heavy layer is higher than that of the lighter layer and therefore the depth of the dense layer must be less than half of the channel to conserve volume [27].

The Froude number characterizes lock exchange flow well because it compares inertial flow to buoyancy, the major characteristics that contribute to density driven flow versus molecular diffusion [1], [22], [23].

Oh and Kim found that for the Reynolds number range of 10,000 to 100,000 for Boussinesq and non-Boussinesq flows, the speeds of the fluid layers are independent of the Reynolds number [27]. They also found that the Reynolds number has no significant effect on the densimetric Froude number [11]. Computationally, Birman, Martin and Meiburg found that the front velocities are independent of the

Reynolds number above 4000 for the low density fluid, which suggests that it is energy conserving over the entire range of Re. The heavy front however, has strong vortexes and dissipates a lot more energy than the light front, suggesting that it acts as a dissipate gravity current in contrast to the light front acting as an energy-conserving gravity current that is closely approximated by theory of Benjamin [24], [28].

Lowe, Rottman, and Linden found that the structure of a dissipative gravity current can be broken up into 3 regions: there is an energy conserving head, a wake region with mixing, and then a uniform tail. This article determined that the head of the current is insensitive to the wake region thus mixing plays a small role in the velocity of the gravity current, giving the current a constant speed although the regions are travelling at three different velocities as can be seen in Figure 4 [29].

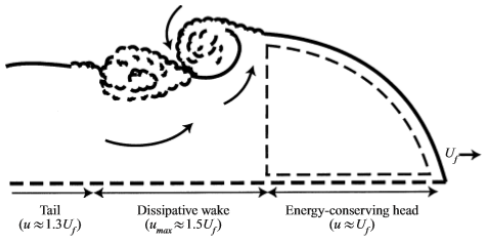

Figure 4: Structure of a dissipative gravity current [29][3]

LRL determined that the density ratio that separates Boussinesq from non-Boussinesq flows is 0.281 [11]. For values of γ from $0 < \gamma \leq \gamma^*$ where $\gamma^* \approx 0.281$, LRL define the velocity of gravity current to be:

$$U = \sqrt{(1-\gamma)gH}\left[\frac{1}{\gamma}\frac{h_H}{H}\left(2-\frac{h_H}{H}\right)\frac{1-{h_H}/{H}}{1+{h_H}/{H}}\right]^{1/2} \quad where\ \gamma = \frac{\rho_{light}}{\rho_{heavy}}$$

The velocity is dependent on the density ratio, gravity, the height of the channel and the depth of the heavy current. The energy conserving head maintains its initial height at around half of the channel even in non-Boussinesq conditions; the measured depth of the current is in the tail region from Figure 4 [11], [28], [29]. Between the head and the tail there are billows, called Kevin-Helmholtz instabilities, that promote mixing and turbulence at the interphase [30]. LRL developed an analytical theory to estimate the channel depth for each density ratio and matched their values with

[3] "Reprinted from Journal of Fluid Mechanics, Vol 456, R. Lowe, P. Linden, and J. Rottman, "A laboratory study of the velocity structure in an intrusive gravity current,", Pages 33-48, 2002, with permission from Cambridge University Press."

experimental and computational results from Birman et al. and others to create Figure 5 and 6 [27], [28].

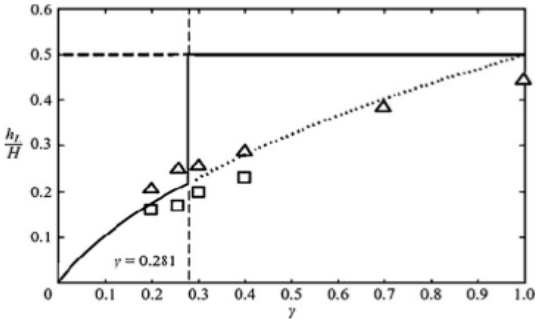

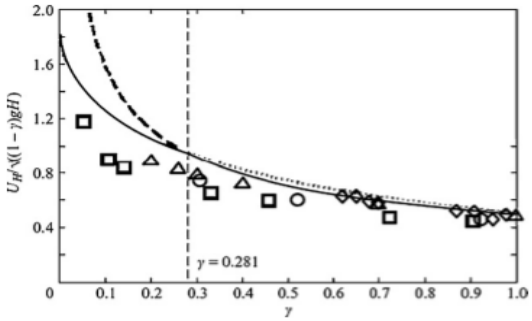

Figure 5: Flow depth of the heavy current [11], [27]
Figure 6: Speed of the heavy current [11], [27] [4]

Oh and Kim then defined the superficial velocities (U_s) of air and helium, depending on the depth of the fluid layer and calculated the air mass flow rate [11].

$$U_s = \frac{Uh}{H}$$

2.3.3 Interphase Stability and Mixing

There are two opposing forces for interphase stability in non-Boussinesq flows. The first is that the larger density difference creates a more stable interphase. However, larger density differences also increase the speed of the heavy fluid, creating more shear stress on the interphase. This regime of flow is called stratified shear flow. LRL confirmed that the interphase is unstable for low and high values of γ as shown in Figure 7 [27].

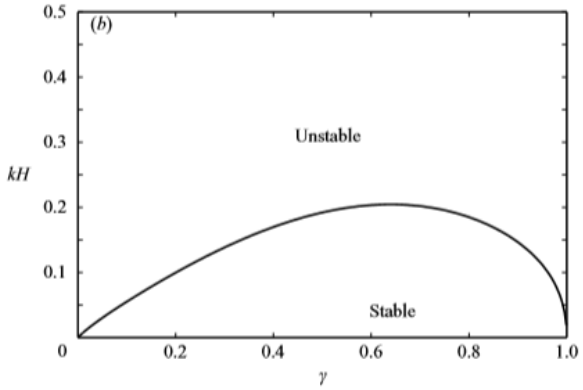

Figure 7: Stability of the heavy fluid interphase [27] [5]
**k in Figure 7 is the wave number of the wave.*

[4] "Reprinted from Nuclear Engineering and Design, Vol 241, Chang H. Oh and Eung S. Kim, "Air-ingress analysis: Part 1. Theoretical Approach", Pages 203-212, January 2011, with permission from Elsevier."

[5] "Reprinted from Journal of Fluid Mechanics, Vol 537, R. Lowe, P. Linden, and J. Rottman, "The non-Boussinesq lock-exchange problem. Part 1. Theory and Experiments,", Pages 101-124, 2005, with permission from Cambridge University Press."

At Reynolds numbers larger than 10,000 a 3D turbulent inertia is generated from the Kevin-Helmholtz instabilities to create a completely homogenous flow close to the interphase [31], [32].

When the Froude number is less than 1, vertical and horizontal motions will cause continuous small scale turbulence along the interphase, even if the Richardson number is more than 1. The Richardson number is the ratio of buoyancy forces to inertial forces. The resulting regions are high shear and have low local Richardson numbers that create a flow susceptible to Kevin-Helmholtz instabilities. Kevin-Helmholtz instabilities are not the only turbulent forms shown to appear in experimental work with strong stable stratification. Billant and Chomaz showed that quasi-horizontal flows can have "zig-zag" instability as well [33]. Current literature for lock exchange flow in MHTGRs in particular cites Kevin-Helmholtz instabilities, however [30]. For these instabilities to occur, the Reynolds number must be large.

Stability of the interphase can be calculated at a function of the Richardson number. Low Ri numbers have little turbulent mixing and rely on diffusion. The Ri number can be defined as a function of the wave frequency and vorticity length or of Froude's number:

$$Ri = \frac{1}{Fr^2}$$

Once the heavy gas front has entered the lower plenum, the posts disrupt the layered flow creating wake, which is experimentally displayed by Holford and Linden by towing vertical bars through stably stratified fluids shown in Figure 8 below [33].

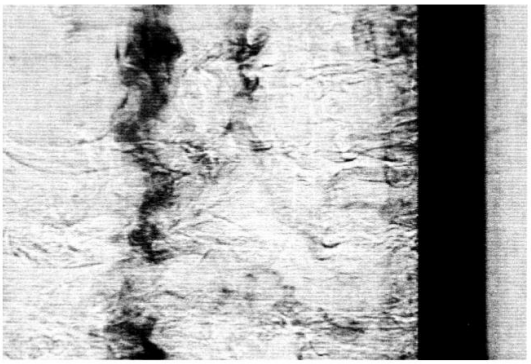

Figure 8: Wake generated behind cylinders dragged through stratified fluids [33][6]

[6] "Reprinted from Dynamics of Atmospheres and Oceans, Vol 30, Joanne M. Holford and P. F. Linden, "Turbulent mixing in a stratified fluid", Pages 173-198, June 1999, with permission from Elsevier."

Fincham, Maxworthy and Spedding found that at low Froude numbers, such as what the HTTF will experience, the strong shear governs the dissipation rate behind the cylinders with quasi-two dimensional vortices [34].

At high Ri, vertical vortices that enhance mixing are released in the wake of the vertical bars as shown in Figure 9 [33].

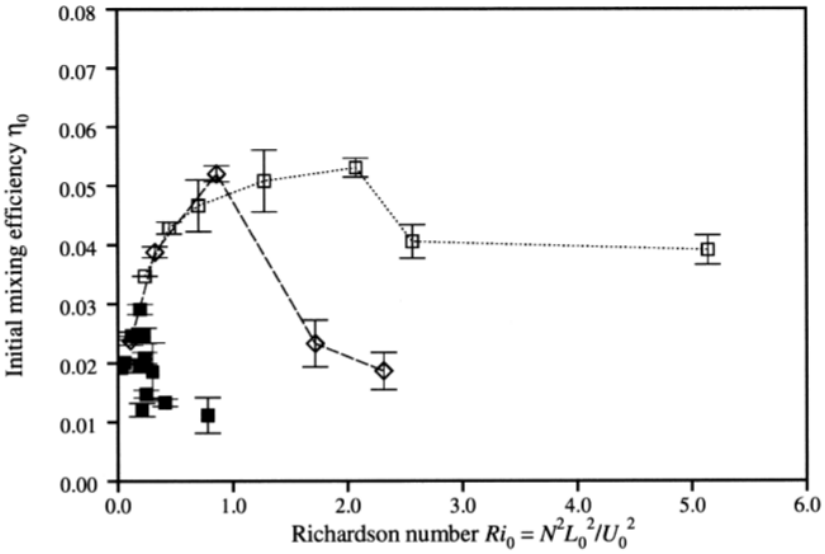

Figure 9: Initial mixing efficiencies in cylinder wake [33] [7]

2.4 Studies directly related to lock exchange flow after DCC Events in a HTGR

As a high priority for research in HTGRs, there are many aspects of lock exchange flow after a DCC event that have already been explored [19]. This section will discuss the results of some of that research.

2.4.1 Lower Plenum Flow

The CFD results of Ham et al. show that the top of the cavity gas plume when entering the lower plenum is about half the height of the cross-duct channel, which agrees with the theoretical gravity current work by Benjamin [24], [35]. Once the air-helium mixture reaches the lower plenum, the plume spreads out to fill radially from the entrance of the hot duct. The diametrical path is a shorter length, however, the support columns introduce hydraulic resistance to the flow so that the flow across the support columns and around the circular edge of the plenum reach the opposite side at

[7] "Reprinted from Dynamics of Atmospheres and Oceans, Vol 30, Joanne M. Holford and P. F. Linden, "Turbulent mixing in a stratified fluid", Pages 173-198, June 1999, with permission from Elsevier."

approximately the same time, as seen in the figure 10 [35].

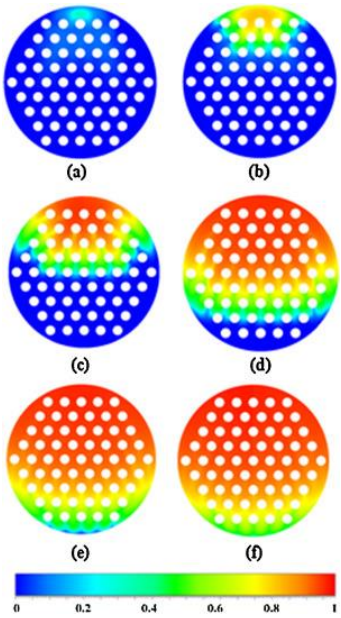

Figure 10: Lower Plenum Flow Patterns over time [16][8]

Oh and Kim also conducted some numerical analyses of the DCC event post depressurization (boundary conditions for after depressurization were calculated with the GAMMA code), with a FLUENT simulation that assumed porous core material and a CFX-12 simulation that used real geometry. Using real geometry is especially important with the complicated geometry in the lower plenum [36], [37]. The CFX simulation matched well with the FLUENT simulation with air filling the lower plenum at 10 seconds in FLUENT, and 9.86 seconds in CFX [37], [38].

In the Oh et al. CFX-12 3D simulation, the air mixture reaches the opposite side of the entrance to the lower plenum at 6 seconds; as the air hits the wall edge, it recirculates, loses momentum and builds pressure inside the core. The air starts travelling up the core blocks at 10 seconds as pressure build-up overcomes the hydrostatic pressure and the lower plenum is filled at 20 seconds [22], [36], [39]. During their simulation, they found that even though 80% of the lower plenum was filled with air at 10 seconds, air did not yet start penetrating the core. They speculated that this is because the helium is still flowing out of the top of the lower plenum or that the buoyancy force of the air is weak compared to the momentum of

[8] "Reprinted from Nuclear Engineering and Design, Vol 288, David J. Arcilesi, Tae Kyu Ham, In Hun Kim, Xiaodong Sun, Richard N. Christensen and Chang H. Oh, "Scaling and design analyses of a scaled-down, high-temperature test facility for experimental investigation of the initial stages of a VHTR air-ingress accident", Pages 141-162, July 2015, with permission from Elsevier."

the helium discharging. The moment the air starts to penetrate the core is visible by studying the volume averaged temperature variation results in the lower plenum and cold duct header shown in the figures below [36], [39].

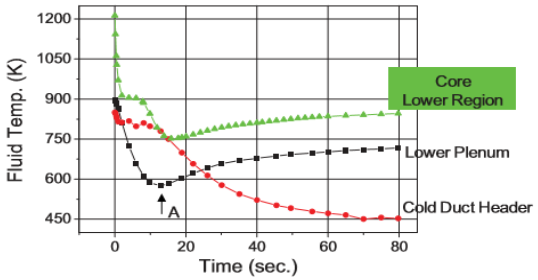

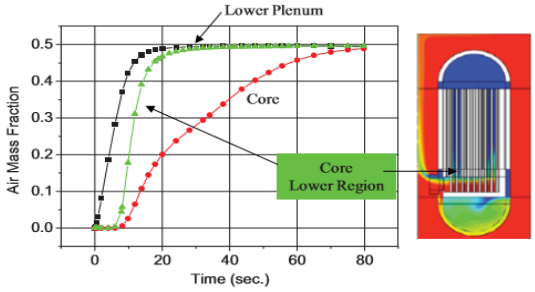

Figure 11 (On the left): Volume and area averaged temperature of various vessel regions [39] [9]
Figure 12 (On the right): Volume and area averaged air mass fractions of various locations in the vessel [39][10]

The A in Figure 11 denotes the start time of air penetration into the core as can be seen in the following Figure 12. Therefore, it is postulated that air heating time by the lower plenum structure and support block is essential for the buoyancy force because buoyancy is dependent on a local value compared to an average value. If the temperature in the lower plenum can be maintained lower, then the onset of natural circulation can be delayed. The 3-D model also confirmed that assumptions in the 2-D model were acceptable, however, the onset of natural circulation in CFX-12 is 100 seconds, half of the value of the 2-D simulation. [22], [36], [39].

Ohio State University is also planning physical experiments on a 1/8th scale in height and diameter of a VHTR specifically to study lower plenum phenomena during accidents [16]. Computationally, during the scaling analysis for Ohio State University's high-temperature test facility, Arcilesi Jr. et al. found that the time for the plume to reach the halfway point of the lower plenum for their scaled facility was 1.85 seconds after the break initiation. The cavity gas front reaches the back of the plenum at 4.1 seconds. The propagation of the cavity gas draws similarities with other CFD analyses by Ham et al. [35] with the gas reaching the other side of the lower plenum at the same time diametrically as circularly around the edge of the plenum because of the increased pressure loss from the lower plenum support columns. Ohio State tests will be performed while maintaining either the air-to-

[9] "Reprinted from Nuclear Engineering and Design, Vol 241, Chang H. Oh, Hyung S. Kang and Eung S. Kim, "Air-ingress analysis: Part 2—Computational fluid dynamic models", Pages 213-225, January 2011, with permission from Elsevier."
[10] "Reprinted from Nuclear Engineering and Design, Vol 241, Chang H. Oh, Hyung S. Kang and Eung S. Kim, "Air-ingress analysis: Part 2—Computational fluid dynamic models", Pages 213-225, January 2011, with permission from Elsevier."

helium mole ratio in containment or the final mixed mean temperature to get a similar boundary conditions for air ingress after the depressurization phase [16].

2.4.2 Sensitivity Analyses

A sensitivity study was conducted on flow regimes for lock exchange flow. The laminar model predicts the most air ingress because there is less mixing thus a larger density gradient between the gas constituents [40].

The blow down phase determines the molecular concentration of helium versus air inside the cavity which contributes greatly to the density gradient between the cavity and the reactor [40], although the density gradient is more sensitive to the change in temperature than molecular concentration [22].

The next sensitivity analysis conducted surrounded flow resistance. They found that an order of magnitude increase in flow resistance only reduces the penetrations of air by 10 to 15%. Thus, flow resistance effects are expected to be negligible [40].

2.4.3 Comparing experimental work with numerical analyses

Oh and Kim conducted isothermal air-ingress experiments to validate computational fluid dynamics software in the Boussinesq regime. Brine and sucrose were used as heavy fluids and water was used as the light fluid with density ratios ranging between 0.98 and 0.866. The experiments were conducted at large Reynolds numbers so that the lock exchange of the fluids can be considered inviscid. They also did a test with water and air with a 0.0012 density ratio. The results matched well within 10% deviation with Benjamin's model [24]. They found that stratification is developed even for cases in which the density differences are not large [5], [41].

Oh et al. created a computer simulation of the Grobelbauer et al. experimental tests to validate their FLUENT code for non-Boussinesq flows [22]. Grobelbauer found that the light gas propagated in agreement with Benjamin's theory with little energy loss. However, there were major differences seen in non-Boussinesq flows seen in the asymmetry of the flow. The heavy gas propagates with energy losses and evidence of mixing behind a raised head, while the light gas head has a smooth interphase [42], [43]. Grobelbauer measured front speeds of heavy intrusions in light fluids as well as light intrusions into heavy fluids. They conducted seven

experiments, with the following constituents in Table 4 [22].

Gases	Density Ratio (ρ_L/ρ_H)
CO_2/argon	0.90
Argon/air	0.72
R22/argon	0.46
R22/air	0.33
Air/helium	0.14
Argon/helium	0.1
R22/helium	0.046

Table 4: Grobelbauer test matrix [22].[11]

In the Grobelbauer experiment with air intrusion into helium, they found the current speed to be 1.25 m/s and the FLUENT simulation calculated 1.19 m/s, showing only a 4.8% error [22], [44]. The data in the first second shows more deviation because of the disturbance from the opening gate in the experimental study, but overall, results the front speeds are constant, suggesting that the inviscid assumption by Benjamin is reasonable [22], [24].

2.4.4 Previous HTTF Work, HTTF DCC pre-test calculations

Utberg conducted a Star CCM+ simulation of the DCC event in the HTTF with various density ratios by changing the molecular masses inside the RCST. He conducted an isothermal and a heated test.

Non-Isothermal Test Case	1	2	3	4	5	6
System Pressure	0 Pa (gage)					
Helium Temperature	687 °C					
Nitrogen/Helium Temperature	20 °C					
RCST Nitrogen Concentration	50%	60%	70%	80%	90%	100%
RCST Helium Concentration	50%	40%	30%	20%	10%	0%
Isothermal Test Case	**1**	**2**	**3**	**4**	**5**	**6**
System Pressure	0 Pa (gage)					
Helium Temperature	20 °C					
Nitrogen/Helium Temperature	20 °C					
RCST Nitrogen Concentration	50%	60%	70%	80%	90%	100%
RCST Helium Concentration	50%	40%	30%	20%	10%	0%

Table 5: Utberg Pre-Test Calculation Test Matrix [9]

Utberg used a laminar model because that was found to give the most conservative results. Utberg found that velocities decrease as the density gradient

[11] "Reprinted from Final Report on Experimental Validation of Stratified Flow Phenomena, Graphite Oxidation, and Mitigation Strategies of Air Ingress Accidents INL/EXT-10-20759, Chang H. Oh, Eung S. Kim, Hee C. No, and Nam Z. Cho, page 113, January 2011, with permission from INL."

decreases. Utberg also found that as the proportion of nitrogen increases in the RCST or the temperature of the reactor is higher, the lock exchange flow accelerates because of more pronounced density differences. The heated test took half the amount of time to achieve natural circulation than the isothermal test, the results of the heated test are tabulated below in Table 6. For the isothermal cases with 50%, 60% and 70% nitrogen/helium mixtures, 120 seconds had not yet fully stratified the gas layers to bring the onset of molecular diffusion. For 80%, 90%, and 100% nitrogen in the cavity versus helium, full stratification was achieved after 89.35, 59, and 36.9 seconds, respectively [9].

	Approximate Time to Fully Developed Thermally Stratified Layer (seconds)
50% Nitrogen/50% Helium:	66.225
60% Nitrogen/40% Helium:	53.75
70% Nitrogen/30% Helium:	42.925
80% Nitrogen/20% Helium:	33.625
90% Nitrogen/10% Helium:	25.3
100% Nitrogen/0% Helium:	17.8

Table 6: Time to form a fully developed thermally stratified layer [9]

Gutowska explains that the depressurization phase is very short. It spans a length of a few seconds until pressure equilibrium is attained. Gutowska found that choked flow occurs when the absolute pressure upstream compared to downstream pressure is equal to or greater than 2.049 and that the mass flow rate during choked flow follows the equations below [15]:

$$\dot{m}_{Brk} = A_{brk} \frac{P_{vessel} \sqrt[2]{\gamma_g * (\frac{2}{\gamma_g + 1})^n}}{\sqrt[2]{CF_{g,vessel} T_{vessel}}}$$

$$n = \frac{\gamma_g + 1}{\gamma_g - 1}$$

The initial conditions for Gutowska's simulations are in Table 7 below:

	Pressure [MPa]	Temperature [K]	Fluid
Vessel (upcomer, upper plenum, MCSS)	0.8	523	Helium
Cavity	0.1	293	Air
Core	0.8	960	Helium
LP	0.8	960	Helium

Table 7: Gutowska initial simulation conditions

Gutowska used assumptions for porous body as the core and also conducted a turbulence sensitivity analysis where the K-Epsilon turbulence model was chosen [15].

Milliseconds after the valve is opened a Riemann shock wave propagates towards the cavity and compresses the gas in the direction in which the wave is traveling. An expansion wave travels in the opposite direction and reflects off the lower plenum back wall. Higher temperatures are seen behind the reflected shock wave. The absolute pressure curve oscillates as a function of pressure build ups and valleys created by flow reversals and rarefaction waves. The oscillations decay as flow reversal momentum decreases with system pressure until the pressure equalizes. Gutowska concluded that no significant gas transfer occurs during depressurization, which is why systems starting at equalized pressures observe very similar results, as indicated in Magnusson's work [14], [15].

In Gutowska's lower plenum results, at 30 seconds, 90% of the lower plenum volume is full. She found that entrance into the lower plenum can occur as quickly as 2 seconds after the beginning of the transient and that the gas starts rebounding from the lower plenum walls at around 3 seconds until around 20 seconds later, which produces a wavy interface that promotes gas mixing as shown in Figure 13 below. As more air enters the lower plenum, the effect is reduced until a quasi-equilibrium state is reached, which is the start of molecular diffusion. It takes about 30 seconds to fill the lower plenum up to the hot duct upper elevation. The nitrogen gas front reaches the middle of the plenum around 2.5 seconds after the beginning of the transient.

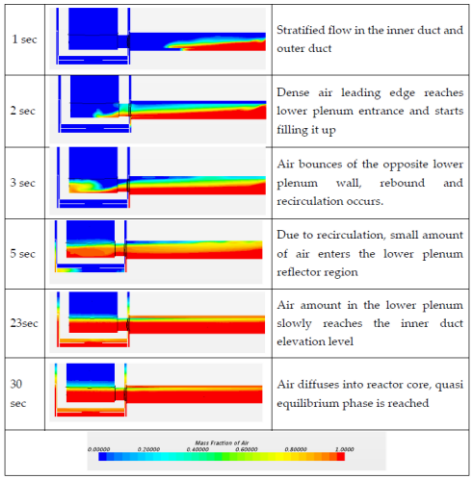

Figure 13: Gutowska's lower plenum visualization results

In Gutowska's results, air concentrations quickly increased in the cross duct and the lower plenum, while concentrations barely decrease in the RCST. Air in the vessel reaches 15% at 30 seconds, however air in the core is only at 0.7%.

Gutowska found that "pure" stratified flow only lasts for the first 6 seconds, before the air wave rebounds off the lower plenum wall, which is 12 seconds in the prototype.

Gutowska concluded that it takes an average of 2 seconds with the cold nitrogen front moving at .45 m/s for the nitrogen gas front to reach the middle of the lower plenum [15]

Magnusson used a simplified geometry of two tanks connected by a tube to simulate lock exchange flow between the PPV and the RCST to study the effects of depressurization on lock exchange flow, the amount of air ingress, and the associated times related to these phenomena [14]. In the model, the RCST is 14.4115 m^3, the vessel is 3.8030 m^3 and the cross duct is 0.2714 m^3. Magnusson conducted three different simulation cases tabulated below:

Case	Air Press (Mpa)	Air Temp (C)	He Press (Mpa)	He Temp (C)	Vessel He %	Blow Down Tank He %
1	0.101325	22	0.101325	670	100	0
2	0.101325	22	0.8	670	100	0
3	0.282697	118	0.282697	634.3	100	15

Table 8: Magnusson Test Matrix

Overall, she found that the ending measurements of gas concentration and temperature are almost the same for the end of Case 2 and Case 3 where there was a depressurization and where the pressures were equalized for conditions after a depressurization respectively. The CFD simulations for Case 2 estimated 82.3% helium in the vessel and Case 3 estimated 81.6 % helium in the vessel. Her tabulated results of times for each case is below:

IC case	Depressurization Completed	Air Enters Vessel
IC case 1	N/A	1.026 sec
IC case 2	0.235 sec	3.000 sec
IC case 3	N/A	2.38 sec

Table 9: Magnusson time results

3. Materials and Methods

3.1 Design of High Temperature Test Facility (HTTF)

The HTTF is mainly comprised of a primary vessel with an electrically heated ceramic block core, a crossover duct between the primary vessel and a RCST. The hot leg is a 12-inch diameter pipe that runs straight from the PPV to the RCST. A 10-inch pipe to the steam generator protrudes upwards from the hot leg 128.91 cm downwards from the outlet of the PPV as shown in Figure 15. 8.5 inches down from the outlet of the PPV is Rake 1 (the small blue circle in Figure 14 below).

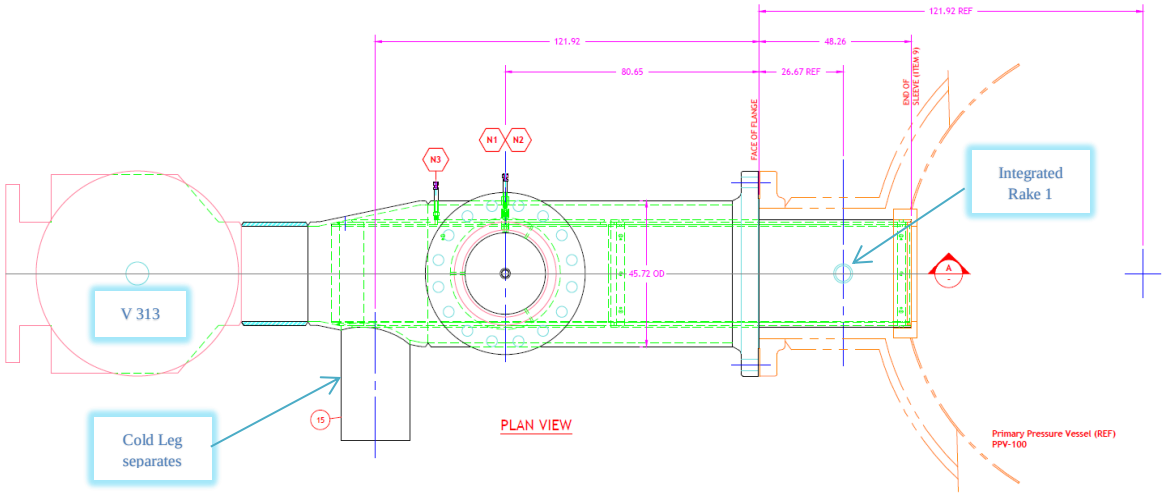

Figure 14: Shows a top down view of the cross duct.

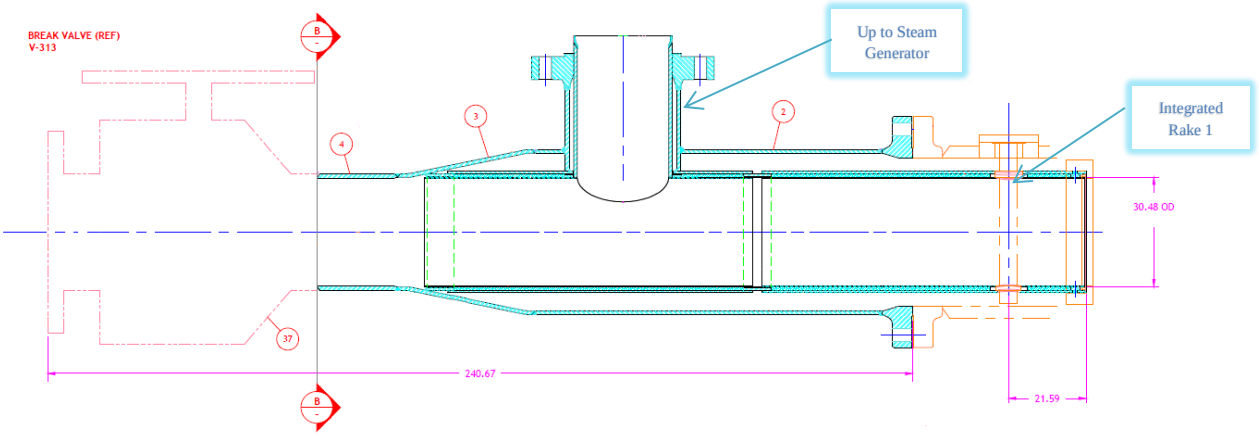

Figure 15: Shows a horizontal view of the cross duct.

The PPV is to the right and the RCST is to the left after the valve V-313 in Figure 14 and 15. The cold leg flows as a shell around the hot leg until it turns to become an independent pipe, marked in Figure 14. The pipe then makes a second 90º

turn to go to the cold leg valve V-311. Nozzle 1 (N1) and Nozzle 2 (N2) in Figure 14 are temperature and pressure nozzles, detailed with an elevated view in Figure 16. Nozzle 1 measures the temperature and pressure in the cold leg and Nozzle 2 measures the temperature and pressure in the hot leg. Nozzle 2 is situated above the duct however, so it does not witness lock exchange flow in the hot duct. Nozzle 3 (N3) in Figures 14 and 16 is a gas fill line for the facility.

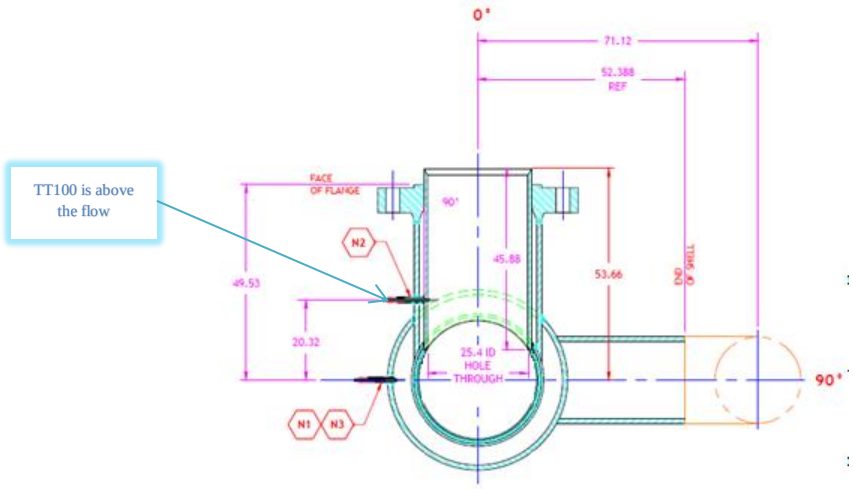

Figure 16: Shows a view down the length of the cross duct.

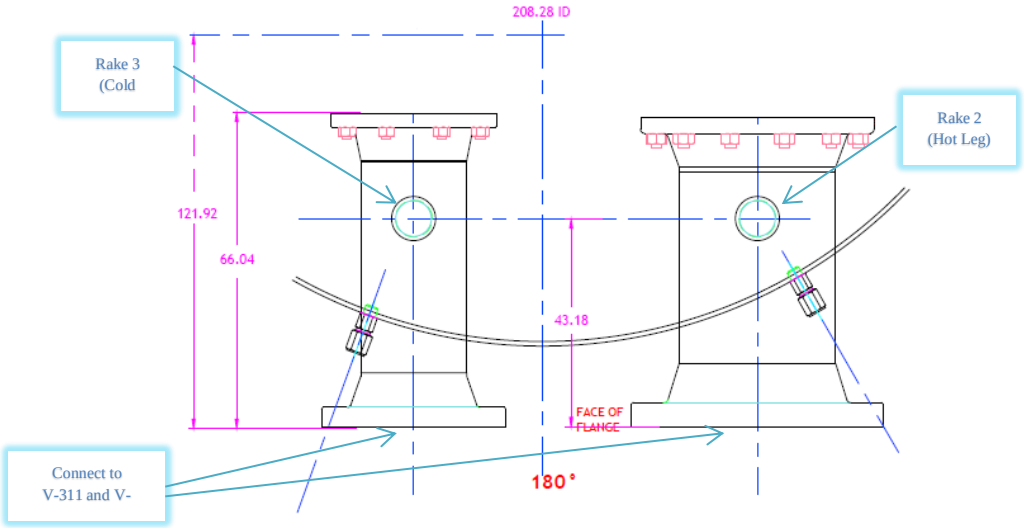

Figure 17: Shows the ducts that travel into the RCST with a top down view.

In Figure 17, the green and black circles represent the locations of Rake 2 and Rake 3. The cold leg is on the left, a smaller diameter pipe, and the hot leg is on the right.

The two main tanks are separated on the hot and the cold legs by two main

break valves. The opening of the two valves is analogous to a DEGB in the MHTGR between the vessel and the steam generator. During normal operation of the HTTF, helium travels through the insulated cold leg, which is the outside shell of the coaxial duct, which further insulates the hot duct. The cold helium gas then travels up the upcomer and turns around to flow downward through the ceramic block core. The lower plenum acts as a manifold and mixes the helium before it leaves the primary vessel through the hot leg. The geometry of the HTTF is shown in Figure 1. The helium would then move through the steam generator and then the circulator to return to the cold leg. The independent cold pipe would then be reintegrated into the cold and hot coaxial duct.

The HTTF operates at prototypical temperatures with an inlet temperature of 259ºC and an outlet temperature of 687ºC. The temperature profile in the core is maintained in the smaller volume by using ceramic core blocks (orientation shown in the figure below), instead of graphite.

Channels description	Channel structure	Height [in]
Core blocks (CB): 6 inner gap 36 outer gap 516 coolant 210 heater rods ($HR^{1,2}$)	CB, HR_1	11″
	CB, HR_1	4″
	CB, $HR_1 \rightarrow HR_2$,	7.8″
	CB, HR_2	7.8″
Lower Reflector 1 (LR1): 36 outer bypass 6 inner bypass 180 coolant 30 Heater rod buss bars (HRB)	CB, HR_2	7.8″
	CB, HR_2	7.8″
	CB, HR_2	7.8″
	CB, HR_2	7.8″
Lower plenum roof (LPR): 6 inner bypass 36 outer bypass 192 coolant	CB, HR_2	7.8″
	CB, HR_2	7.8″
	CB, HR_2	7.8″
Lower Plenum: 163 posts	CB, HR_2	7.8″
	CB, HR_2	4″
	CB→LR1, HRB	4″
	LR1→LPR	4″
	LPR→LP	7.8″
$HR^{1,2}$ – 1 and 2 efers to different placement or rods	LP, HRB	14″
	-	3.125″

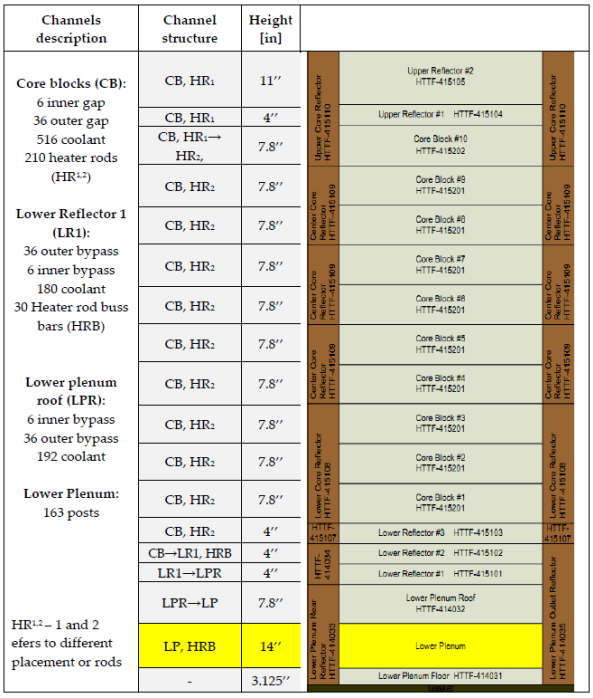

Figure 18: Core block orientation.

Although the core is not made of graphite, graphite heaters are used because the resistive heat produced does not change significantly with temperature [15]; thus, nitrogen is used instead of air in the experiments. The HTTF is scaled one-fourth in

diameter, one-fourth in height and one-eighth in pressure of the MHTGR. The facility is unable to undergo a full depressurization as would occur in the MHTGR. Pre-test calculations have been conducted to suggest that a depressurization would have little effect because the blowdown would take less than 1 second [14].

In addition to the change in scale, the core is not prototypical shown in the geometry of the lower plenum in comparison to the hot leg in Figure 19 below. Generally, the lower plenum floor would be below the entrance to the hot duct and roof would correspond to the height of the hot duct; in the HTTF the hot duct in a 12-inch diameter pipe. The lower plenum is only 8.75 inches tall, and the plenum floor lines up with the bottom of the pipe, and the lower plenum roof sits below the top of the hot leg pipe, as shown in the figure below. This change was caused by the fact that the flow paths were scaled by flow area and the PPV was scaled by height [12].

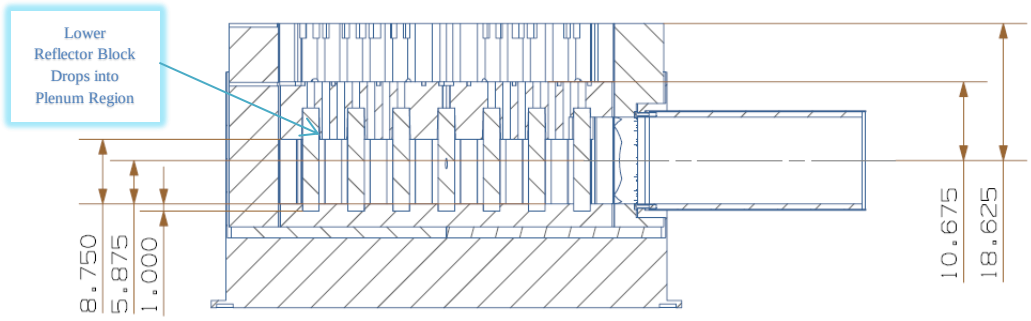

Figure 19: Lower Plenum geometry in comparison to the outlet of the hot leg pipe.

The change of geometry will present a higher amount of hydraulic resistance and form loss in the lower plenum as it fills, however, an increase in hydraulic form loss by one order of magnitude only contributes 10%-15% decrease in lock exchange flow speed [40]. The floor of the lower plenum sits flush with the bottom of the hot duct pipe therefore there is no drop for the nitrogen to experience going into the lower plenum. This may maintain the nitrogen front integrity for longer time while travelling into the core than if there was a drop to create turbulence and mixing.

3.2 Description of the Experiment

The purpose of this experiment is to observe the impacts of changing the initial conditions, including a depressurization, of the PPV and the RCST on lock exchange flow. By changing temperatures, pressures, and gas concentrations the density gradient between the two tanks can be changed. The density gradient is the

driving mechanism of lock exchange flow.

Utberg's pre-test calculations changed the gas-composition inside the RCST to change the density gradient between the two chambers for two case temperatures of isothermal and normal operating condition temperatures [9]. If the density gradient remains the same, any gas can be used and validated with this experimental data.

The end of lock exchange flow is the creation of a stable thermally stratified layer in the lower plenum. Noted as a quasi-equilibrium state, stratified layers of nitrogen and helium are formed, heated expansion and molecular diffusion will be responsible for transporting the air up into the core. The time scale for achieving a stable thermally stratified layer is within minutes of opening the break valves as suggested by Utberg [9].

The experimental procedure requires that first the temperature of the core is adjusted and well mixed to ensure a stable temperature profile. The RCST also experiences thermal stratification and thus must also be mixed before tests are conducted. This experimental test matrix is below as Table 10:

Test #	1	2	3	4 →(depressurization)→4	5*
Plenum Temp** [ºC]	20±2	19.5±2	17.1±2	90±2→150±2	160±2
PPV Gas	He	He	He	$He+H_2O$→ N_2+He+H_2O	$He+H_2O$
RCST Temp** [ºC]	20.5±2	20.5±2	18±2	18±2→41±2	19±2
RCST Gas	N_2	N_2	N_2	N_2→ N_2+He+H_2O	N_2
PPV Pressure [kPa]	99±.99	100±1	116±1.2	404±4.04→160±1.6	107±1.1
RCST Pressure [kPa]	99±.99	100±1	116±1.2	77±.77→160±1.6	107±1.1
Cold Leg Opened?	No	Yes	Yes	No	Yes

Table 10: Initial Conditions for the DCC Experimental Matrix
**Concentration of H_2O unknown*
***Represents Average Temperatures (Plenum temperature is not necessary the same as core average)*
****4 after are the initial conditions for lock exchange flow after depressurization*

Note from in the test matrix, the plenum temperature is not always the same as the core average because it depends on if the PPV is well mixed before the DCC is commenced. In several of the tests, the PPV was not mixed immediately prior to the accident which leaves stratification inside the vessel. For DCC 4 the core was also still heating.

If the RCST and the PPV are not yet pressurized with the correct gases the system must be evacuated of air and filled with helium and nitrogen gas. The tanks are vented to atmospheric and refilled with the desired gas until oxygen levels are less than 1% in the facility. The circulator is turned on to mix the gas in the primary system. Then the heaters are enabled and turned on until the thermocouples in the crossover duct reach the desired temperature. The heaters and the circulator are turned off and the circulator is isolated from the DCC event. Immediately before the actuation of the main break valves, the blower for the RCST is turned on to mix the thermally stratified nitrogen tank, however this did not occur in any of the tests except for DCC 2.

For the tests with equalized pressures, the primary and the RCST pressures are equalized utilizing vent valves and the upper break valve between the two tanks right before opening the two main break valves to ensure that the tanks are the same pressure and that there will be no blow down. The hot leg valve is opened (V-313), which takes 14 seconds. The cold leg valve (V-311) is opened roughly 6 seconds after the hot leg valve, which takes about 10 seconds to fully open.

The hot leg pipe inside the RCST was extended to the middle of the RCST. The extension of the hot leg pipe in the RCST is suspected to have a negligible effect on the lock exchange flow. The extended distance will allow for better confidence that the nitrogen gas front is stable before reaching the RCST thermocouple rakes. The thermocouple in the RCST are situated behind the outlet of the pipe and thus the temperature influenced by the intruding helium in RCST may have a slightly delayed response.

Each test has slight deviations from the procedure. In DCC 1 and DCC 4, the only valve that was opened was the hot leg.

In DCC 4 the PPV pressure was vented to an appropriate pressure as to not exceed the safety valve limitations of the RCST pressure. Additionally, the core was still heating and the circulator had been turned off for twenty minutes allowing stratification of helium in the core. DCC 5 was also stratified.

3.3 Instrumentation

The HTTF has several instruments that will measure lock exchange flow

phenomena. There are thermocouples inside the lower plenum, the cross duct, and the RCST.

In the RCST, the thermocouples are installed at 3 different heights: 83.8, 350.8 and 526.4 cm vertically. The thermocouples are located 180º from the middle of the outlet of the cold and hot legs. They will be used to watch the general stratification of the RCST and to measure the average temperature inside the tank.

The lower plenum has sixteen instrumented posts out of 163. Four of the posts have only two thermocouples: at 25% height and 75% height, while twelve of the posts have thermocouples at four heights: at the lower plenum floor, 25% height, 75% height and the gas inlet. The thermocouple orientation is shown in figure 23.

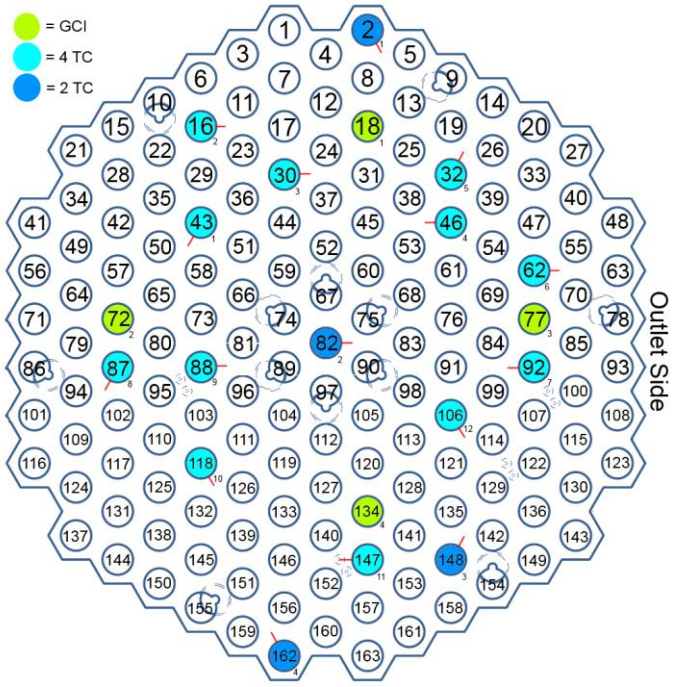

Figure 20: Instrumentation in the Lower Plenum [13]

An additional effect of the lower plenum geometry not matching the height of the hot duct means that the thermocouple heights in the hot leg rakes do not match the heights of the thermocouples in the lower plenum posts. The hot leg rakes have thermocouples at 25% height, 50% height, and 75% height. However, the 25% height and the 75% height in the rake do not correspond to the same percentage heights inside the lower plenum. The 75% height in the lower plenum is at about the 50% height of the hot leg rake.

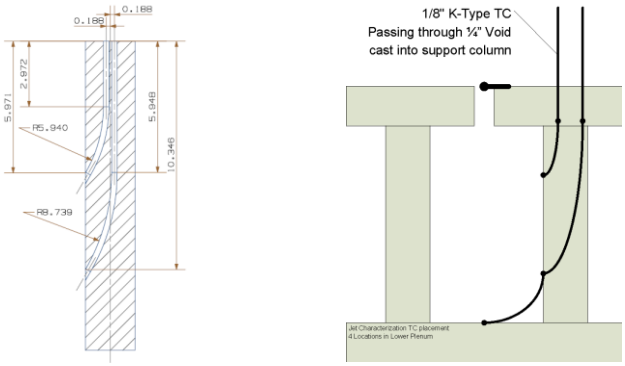

Figure 21: Shows a lower plenum post with thermocouples heights measured.
Figure 22: Shows the orientation of the thermocouples for the lower plenum posts that have 4 thermocouples.

The orientation of the coolant channels shown in Figure 23 is especially important when studying the flow pattern created during the depressurization of DCC 4. Most simulations ignore the jagged edges where the core blocks fit with the side reflectors, this is where flow could bypass the post 2 and post 162 thermocouples or the edges could disrupt the suspected flow pattern of the plenum gas front to move along the edges of the core faster than through the lower plenum posts because of hydraulic form losses. The inlet and outlet can also be seen in the image below. The cold leg does not have a direct path into the core; it gains access to the core by going up through the upcomer and into the upper plenum. The upcomer is instrumented at various heights as well, which will be shown in the results for the heated tests DCC 4 and 5.

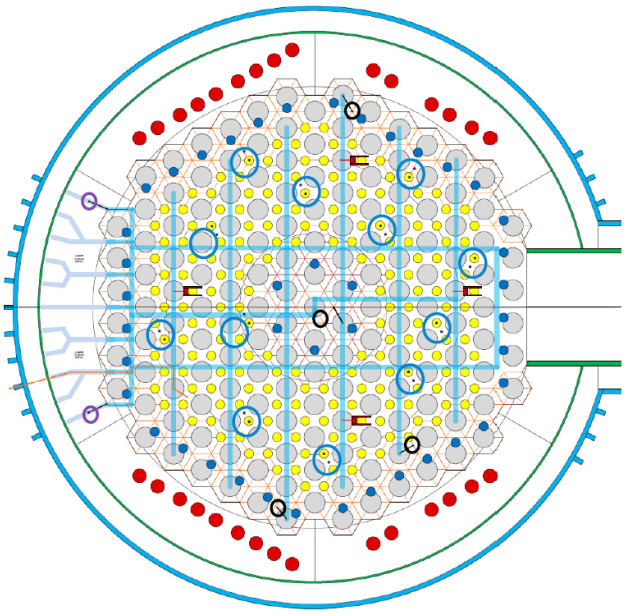

Figure 23: Shows the lower plenum with posts, coolant channels, and heater rods.

From Figure 23, the red circles are the 1.5-inch graphite heater rods. The yellow circles are the 182 one inch diameter coolant channels. The blue circles are the one inch coolant bypass channels in the center. The blue hollow circles are the posts with 4 thermocouples per post. The black hollow circles are the posts with 2 thermocouples per post. The purple empty circles are the reflector temperature thermocouples. And the red capacitor symbols are Gas Concentration Instruments (GCIs).

There are three rakes in the HTTF, although rake one goes through both the hot and the cold leg in the coaxial duct near the PPV so the rake is separated into hot leg rake one and cold leg rake one in the results section. Two of the rakes are shown below, rake two and rake three, which are close to the RCST.

Figure 24: Shows Rake 2 inside the hot leg with thermocouples in the upper, middle and lower regions of the pipe and V-313, the hot leg ball valve, in the background.
Figure 25: Shows Rake 3 inside the cold leg with thermocouples in the upper and lower regions of the pipe and V-311, the cold leg ball valve, in the background.

The rakes will be able to measure the temperature of the gas travelling at various heights inside the cold and hot ducts. For the heated tests the difference in temperature between the RCST and the PPV is large enough to see a distinct difference between the fronts. Then regions of turbulence behind the front and interphase mixing between the helium and the nitrogen may be visible. With the turns present in the cold leg, it is suspected that there may be mixing and turbulence

interrupting the gas fronts.

There were several thermocouples that were not working during various tests. For the first two tests, a CompactRIO (cRIO) failed in the Data Acquisition System which caused thermocouples from posts 87, 88, 118, and 147 to not record data. A full list of thermocouples and those that were not working can be found in Appendix A [13].

3.3.1 Instrument Error

The K-type thermocouples are within 2ºC. This error represents the accuracy of the reading. However, the thermocouples are very precise, so while DCC 1, 2, and 3 were conducted within the range of error of the instruments as shown in the test matrix table 10, the trends and behaviors they observe are real. For example, a thermocouple that measures 25ºC, could realistically be between 23ºC and 27ºC, but its decrease from 25ºC to 24.5ºC does represent a real .5ºC decrease, no matter the initial reading [13]

The systematic uncertainty in the K-type thermocouples at 2.02%. The systematic uncertainty in the static pressure sensors and the differential pressure sensors are 1.26% and 0.78% respectively [13]

4. Results

With the slight temperature differences between the PPV and the RCST during DCC 1, 2, and 3, confidence in the results and resulting hypotheses are low because the differences in temperature are not large enough to distinguish from calibration error. Thus, most of the results will be focused on DCC 4 and 5. Table 11 below displays the parameters of flow for each test and their uncertainty (Table 12).

DCC Test	Channel depth (m)	Gamma	Velocity (m/s)	Superficial Velocity of N2 (m/s)	Superficial Velocity of He (m/s)	Re of N_2	Re of He	Overall Re	Froude of N2	Richardson of N2
1	0.04	0.14	2.24	0.27	1.97	6.37E+05	1.58E+07	3.83E+07	0.45	4.98
2	0.04	0.14	2.23	0.27	1.96	6.43E+05	1.59E+07	3.82E+07	0.45	5.00
3	0.04	0.14	2.23	0.27	1.96	7.57E+05	1.87E+07	3.82E+07	0.45	4.99
4	0.05	0.22	1.73	0.28	1.46	6.43E+05	9.99E+06	2.97E+07	0.40	6.20
5	0.03	0.10	2.93	0.29	2.64	6.33E+05	1.19E+07	5.02E+07	0.54	3.48

Table 11: Analytical Reynolds numbers and stability numbers for the experimental flows derived from pressures and temperatures.

DCC Test	Gamma Uncertainty (%)	Velocity Uncertainty (%)	Superficial Velocity of N2 Uncertainty (%)	Superficial Velocity of He Uncertainty (%)	Re of N2 Uncertainty (%)	Re of He Uncertainty (%)	Overall Re Uncertainty (%)	Froude of N2 Uncertainty (%)	Richardson of N2 Uncertainty (%)
1	0.98	0.57	1.86	0.39	3.76	1.36	0.04	1.85	0.09
2	0.98	0.56	1.83	0.39	3.76	1.37	0.04	1.86	0.09
3	0.98	0.57	1.87	0.39	3.81	1.18	0.05	1.90	0.09
4	0.42	0.58	1.92	0.33	8.54	1.74	0.03	1.92	0.05
5	0.84	0.44	1.43	0.33	3.47	1.88	0.02	1.44	0.10

Table 12: Uncertainty in % of the Reynolds and stability numbers.

Error propagation was calculated in quadrature [45]. The velocity was calculated in the cross duct using equations by LRL in the Boussinesq vs. non-Boussinesq flows section in the literature review, and then the subsequent superficial velocities and Reynolds numbers [11], [27]. The overall Reynolds number is high, suggesting that viscous effects are negligible [11]. High Reynolds numbers with large buoyancy differences experience stratified shear flow, where the flow

interphase is unstable and mixing occurs [32]. The low Froude numbers suggest that the stratified shear flow will have large dissipative wake behind the cylinders in the lower plenum [34].

4.1 DCC 1, 2 and 3

DCC 1, 2 and 3 were ambient tests with the RCST about 1°C hotter than the PPV. In DCC 1, the cold leg valve was not opened, while the cold leg was opened for DCC 2 and 3. Rake 2 and Rake 3 are situated behind the cold and hot leg break valves, measuring lock exchange flow closer to the RCST. The rake one thermocouples are situated in front of the break valves 8.5 inches from the entrance to the PPV shown in the drawings in the Materials and Methods section.

In each of the following plots the hot leg is opened at 1 minute to display steady state before the experiment.

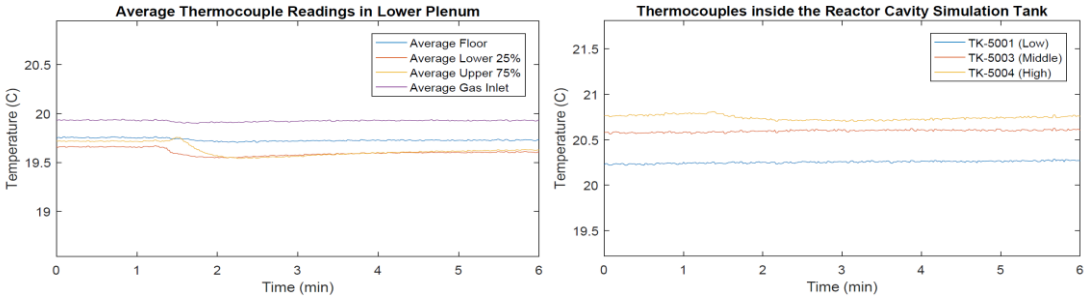

Figure 26: DCC 1 temperatures in the lower plenum and the RCST.

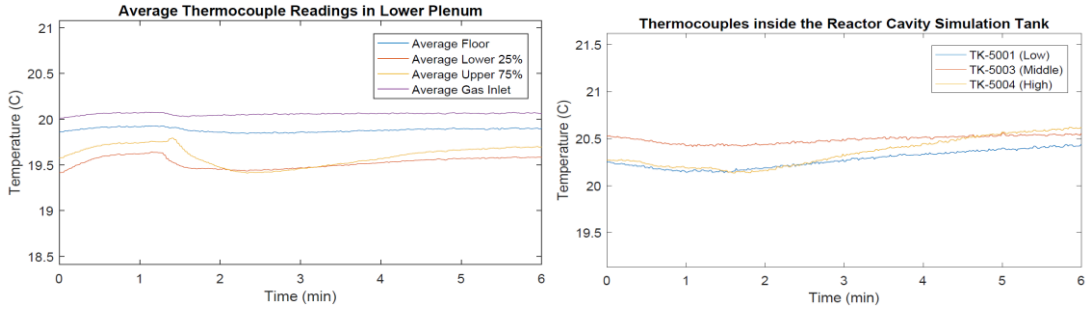

Figure 27: DCC 2 temperatures in the lower plenum and the RCST.

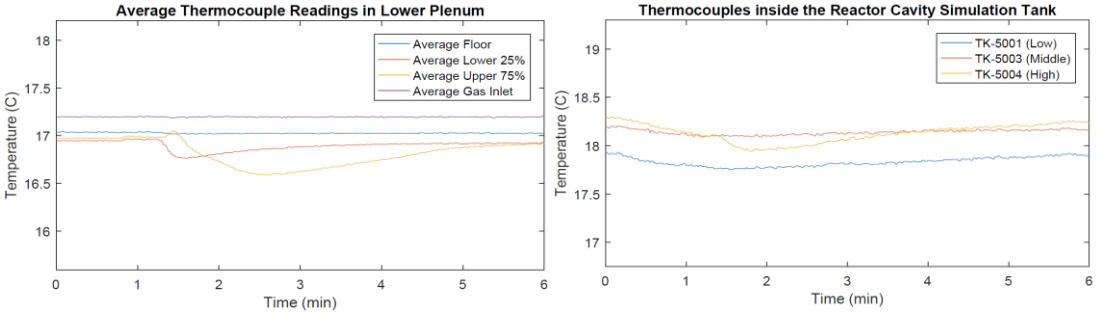

Figure 28: DCC 3 temperatures in the lower plenum and the RCST.

The average thermocouple readings in the lower plenum are created by averaging the temperatures of all the thermocouples at that corresponding lower plenum post height.

Generally, the highest RCST thermocouple decreases in temperature slightly as the helium travels up to the top of the tank and the RCST starts to re-stratify quickly. The volume of the RCST is much larger than the PPV. The other thermocouples in the RCST are mostly unaffected by the cold helium. As an average in the lower plenum the upper thermocouples increase as nitrogen intrudes into the bottom.

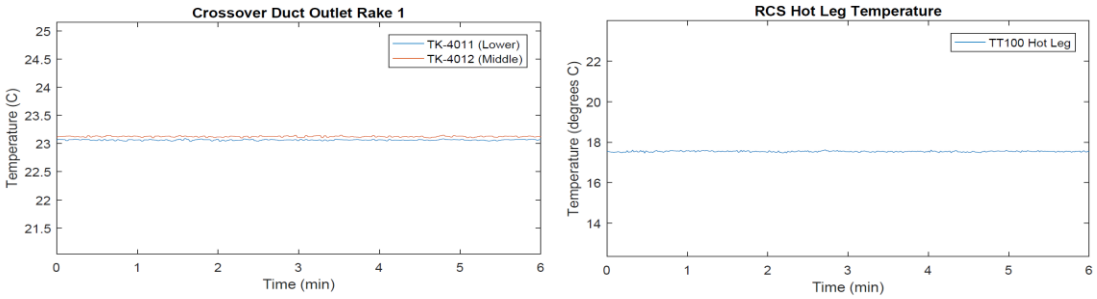

Figure 29: DCC 1 Rake 1 and TT100. Cold Leg unopened.

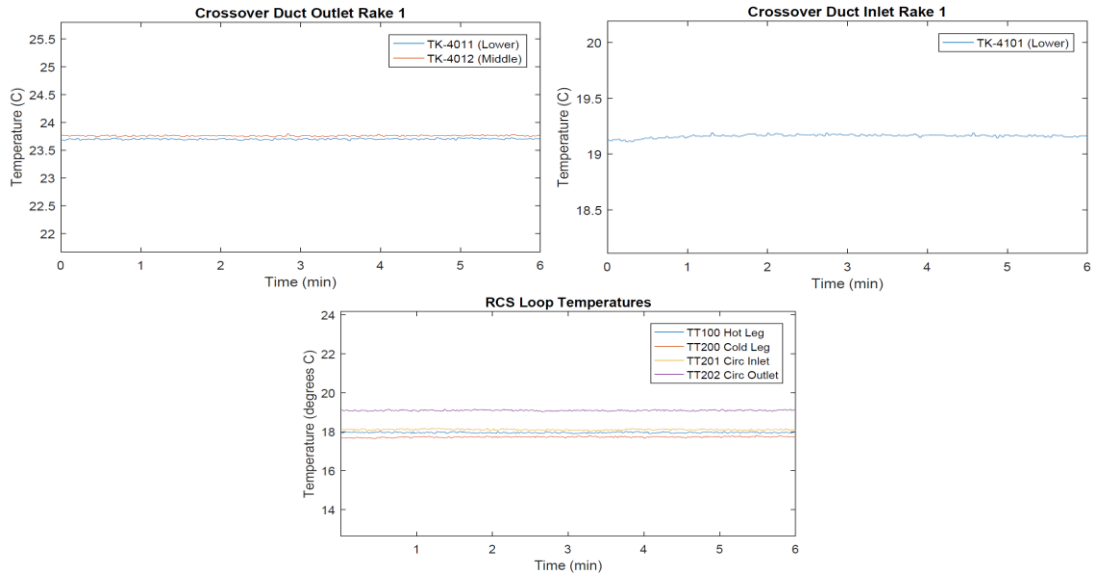

Figure 30: DCC 2 Integrated Rake 1 and TT100.

Figures 29 and 30 show rake one, which is close to the PPV and should read temperatures similar to those in the lower plenum and TT100, which sits nearby, however the temperature of rake one is much higher in DCC 1 and 2 than TT100 and rake one does not observe lock exchange flow phenomena. As shown in the figure, in DCC 2, the lower plenum on average is around 20.5°C, while the rake is reading

temperatures at 23.75°C. The hot leg loop temperature TT100 reads about 19°C, which is much closer to plenum temperatures. The measurement for TT100 is taken at Nozzle 2 indicated in figures from the drawings in the Materials and Methods section. Although these thermocouples seem as if they are not working, they do show temperature change over a longer period of time and are working in DCC 3, 4, and 5. DCC 1 and 2 were the only tests that underwent evacuation for gas filling, which would increase the temperature, and they are the only tests for which there was a cRIO failure for an unknown reason.

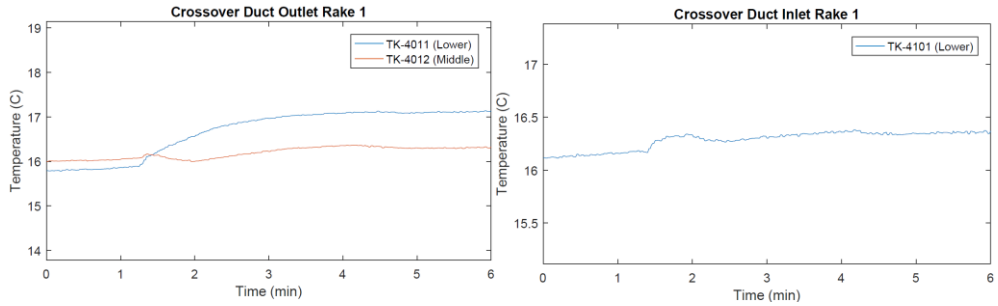

Figure 31: DCC 3 Integrated Rake 1.

In the hot leg, the lower thermocouple increases because it is measuring nitrogen arriving from the RCST. The middle thermocouple rises slightly as it measures the interphase of the nitrogen gas front and then it is unclear if it is measuring the helium after a turbulent area of the nitrogen gas front, or an interphase of mixing, or if the nitrogen has decreased in temperature through heat transfer and it is measuring a lower temperature of nitrogen. The middle thermocouple increase could also be due to rake interference with the gas front. The rake would cause an upward displacement of nitrogen as the front gathers behind the rake with because of flow resistance.

In the cold leg, the lower thermocouple measures the nitrogen intruding into the bottom of the pipe.

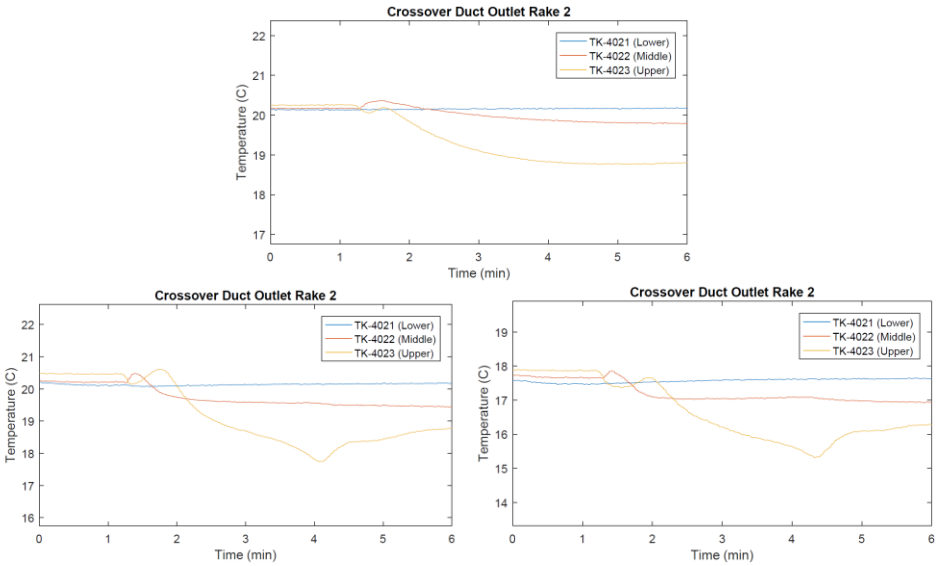

Figure 32: DCC1 rake two measurements of the hot leg near the RCST
Figure 33: DCC2 rake two measurements of the hot leg near the RCST
Figure 34: DCC3 rake two measurements of the hot leg near the RCST

Rake 2 show in the above figures already filled with stratified nitrogen gas and the thermocouples in those rakes will see a decrease in temperature as the helium flows and displaces the nitrogen from the top of the pipe.

LRL found that the less dense gas will travel faster than the dense gas, thus the layers do not share the pipe equally at the halfway point. Instead the denser gas has a smaller layer than the less gas at the top of the pipe [27]. Once the valve is opened, nitrogen continues to flow undisturbed along the bottom of the pipe. It is postulated that helium first encounters the upper thermocouple of rake two, lowering its temperature. As the helium travels, it displaces nitrogen that was stratified at the top of the pipe, pushing it down into the middle of the pipe. The middle thermocouple observes the nitrogen and as the helium layer grows and mixing occurs between the two gases causing the temperature of the middle thermocouple to decrease. The upper thermocouple temperature increases shortly after the helium head arrives displaying possible turbulence and instability behind the helium front head, which research has shown should have a smooth front, demonstrating an inconsistency which is suspected to the caused by a rake interaction.

The inversion of the flow around for DCC 2 and 3 in rake two around 4 minutes suggests that the flow of helium has stopped or decreased and the lower

plenum has been filled or met the bottom of the lower reflector core block, reducing the ease of flow from the core to the duct.

With the very similar behavior between DCC 2 and 3 for rake two, it is suggested that rake one in DCC 2 should have looked like rake one in DCC 3 in Figure 31.

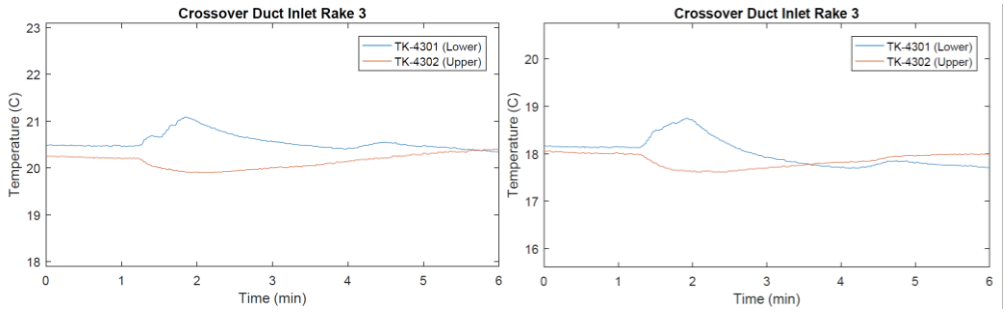

Figure 35: DCC 2 rake 3 measurements of the cold leg near RCST
Figure 36: DCC 3 rake 3 measurements of the cold leg near RCST

Inlet rakes are only shown for DCC 2 and 3 because the cold leg was not opened for DCC 1. It is postulated that the upper thermocouple is at first measuring an intermediate temperature from the temperature stratification of nitrogen inside the cold leg pipe. The helium gas front then meets the upper thermocouple and decreases its temperature, slowly increasing as heat transfer and mixing occurs between the two fluids. The lower thermocouple increases as the helium pushes stratified nitrogen downwards and then the front has turbulence behind the head and further increases. The temperatures then start to come together again after mixing and heat transfer occurs. Like rake two from the hot leg side, there is a change in temperature around 4 minutes, further confirming that some phenomenon is occurring, like a shift from lock exchange flow to molecular diffusion after the complete filling of the lower plenum or filling up to the bottom of the lower plenum reflector block.

4.1.1 Lower Plenum Results

With such similar temperatures in the lower plenum and the RCST, flow analysis in the lower plenum was limited, as 1°C falls into the error of the thermocouple instrumentation. Additionally, the cRIO failure during DCC 1 and DCC 2 disallowed the collection of data from 4 lower plenum posts, further reducing lower plenum data. A few of the working posts during DCC 2 are shown below as an

example of the temperature trends experienced in the lower plenum for the ambient pressure equalized tests.

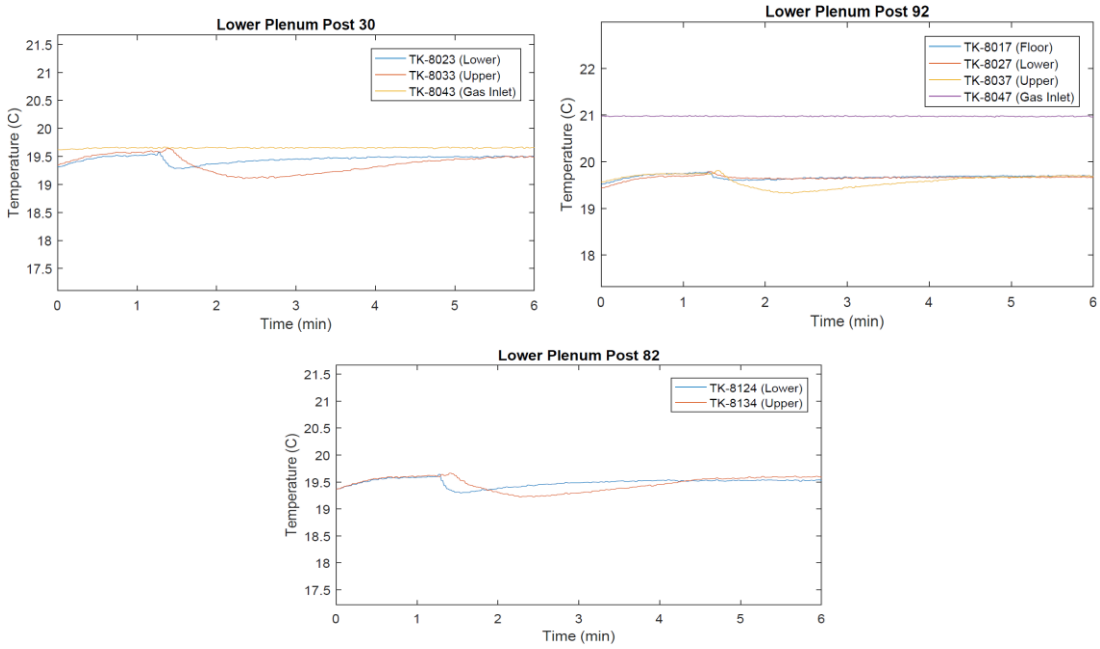

Figure 37: DCC2 Post 30
Figure 38: DCC2 Post 92
Figure 39: DCC2 Post 82

The post orientation can be seen in Figure 20. In post 30, the upper and lower thermocouples experience gas front interaction around the same time. The lower thermocouple first observes a small increase in temperature and then a decrease as it is suspected to be detecting the gas front and subsequent turbulence behind the head. The upper thermocouple experiences an increase in temperature with the helium gas front.

Post 92 observes change in the floor, lower and upper sections of the rod with a small increase and it is speculated that it then observes turbulent mixing because of its proximity to the outlet.

Post 82 is in the center of the PPV. The lower thermocouple experiences a more abrupt change as the gas front arrives. The 3 second delay between the lower and upper thermocouple responses may be due to a bouncing effect of the gas front off the back wall of the plenum and up into the upper level of the plenum.

4.2 DCC 4

The initial conditions for lock exchange flow can be found in Table 10. In

each one of the graphs the hot leg valve is opened at 1 minute to show the steady state conditions before the experiment has initiated. In DCC 4, unlike the other tests, data is collected from the instruments at 2 Hz instead of 1 Hz.

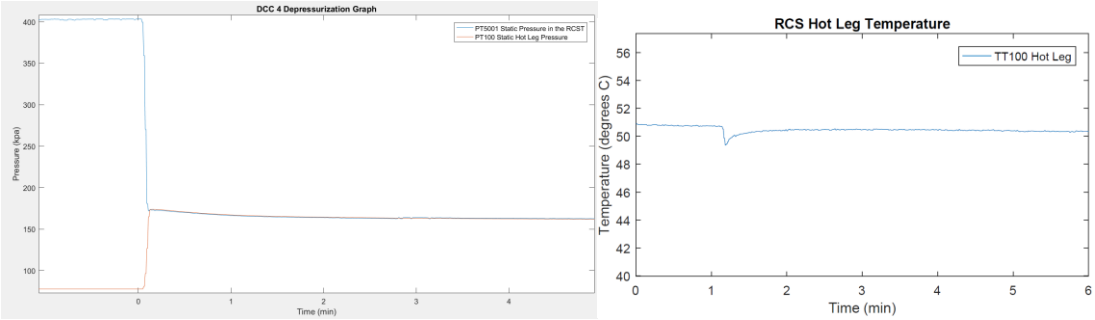

Figure 40: The figures above show the pressure changes during DCC 4.
Figure 41: Shows the cooling effect of the expansion of the gas in the hot leg.

In the figures above, a depressurization from approximately 404 to 160 kPa can be seen. TT100 measures the temperature in the hot leg above the hot duct going into the steam generator. It does not see the effects of the lock exchange flow, but does demonstrate the cooling effect of the gas expansion from the depressurization.

An ideal depressurization of only helium and nitrogen in the system should result in an equalized pressure depending on the concentration and temperature of constituents in each of the tanks as the figure shows below.

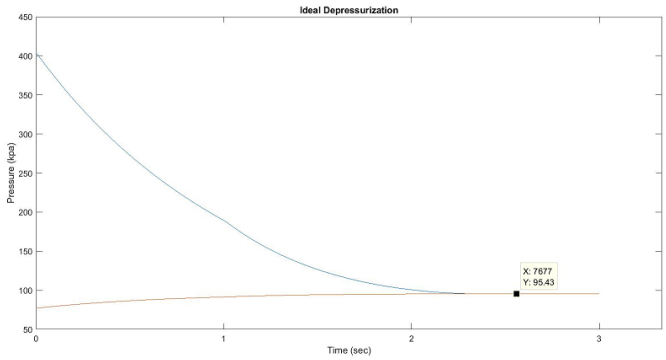

Figure 42: Ideal depressurization of pure helium PPV into pure nitrogen RCST should result in the tank pressures demonstrated above.

However, this was not an ideal depressurization. It is believed that water had been absorbed in the ceramic core blocks, which flashed the steam as the pressure dropped. The superheated steam in the core raised the density in the vessel and increased the equilibrium pressure by 65 kPa after blowdown. The steam and helium were most likely stratified inside the vessel because the circulator had been turned off for 20

minutes prior to the experiment; thus, it is suspected that a large portion of the steam would depressurize into the RCST, which would raise the density gradient between the two tanks thereby accelerating lock exchange flow. Depressurization is vital to setting appropriate boundary conditions when simulating lock exchange flow.

Temperature boundary conditions were also changing simultaneously. DCC 4 is the only test when the core was still in the process of heating, as shown by the side reflector figure below. The heaters were off, but the core blocks were still warming.

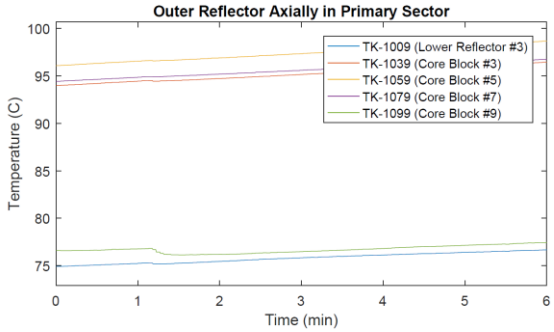

Figure 43: Outer Reflector Temperature Profile Axially.

Without the circulator active immediately prior to the experiments, the helium would not be flowing down the coolant channels and mixing well in the lower plenum and the core would be stratified, as can be seen in the axial upcomer figure below.

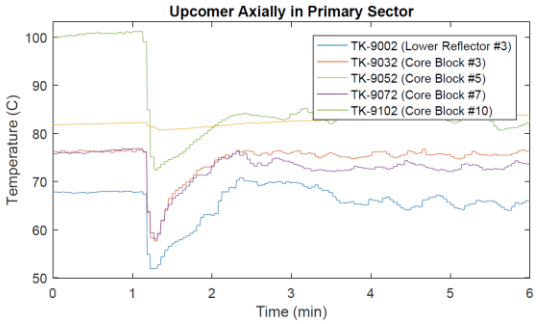

Figure 44: Upcomer Stratification and gas cooling from expansion.

Overall, the general state of the HTTF before DCC 4, was that the core was heating, stratified and at 404 kPa with steam in the primary system. The core was then depressurized into the RCST, where the gas expanded, lowering the temperature in TT100 from Figure 41. The expansion travelled up the upcomer into the upper plenum. Expansion in the upper plenum forced hot gas down through the core into the lower plenum as can be seen in Figure 54. The lower plenum temperature

increased and the increased temperature travelled out of the hot leg past the thermocouple rakes and into the RCST, where the temperature also increased. The temperature increase and movement is due to the expansion of the gas and the momentum driven response of the system to a depressurization.

The change in pressure of the PPV into the RCST experiences choked flow, as the absolute upstream pressure of helium compared to the downstream pressure of nitrogen is greater than 2.049 [15], depressurizes quickly, but residual temperature effect persists and influences the initial conditions of lock exchange flow.

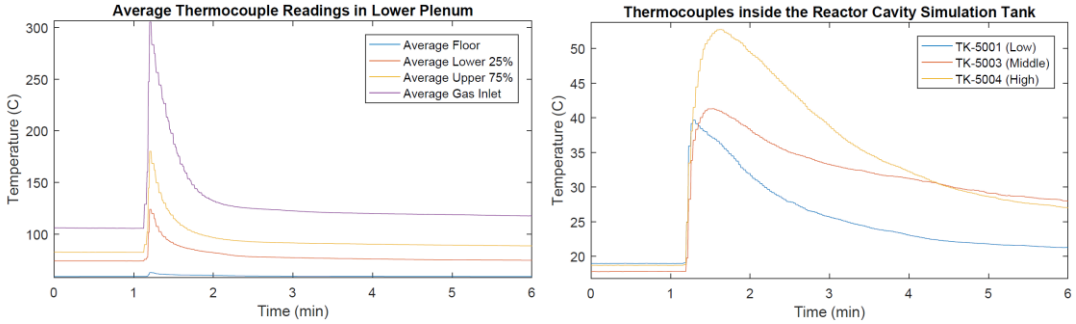

Figure 45:Average lower plenum temperatures during DCC 4
Figure 46: RCST temperature profile for DCC 4.

The higher lower plenum temperatures create a larger temperature difference and thus a larger density gradient for the lock exchange flow to act upon. The RCST temperature also increased.

The hot leg rakes see an increase in temperature as the helium is pushed out of the lower plenum into the RCST as a reaction to the depressurization in Figure 47. As can been seen in rake one, the lower thermocouple decreases around 110 seconds.

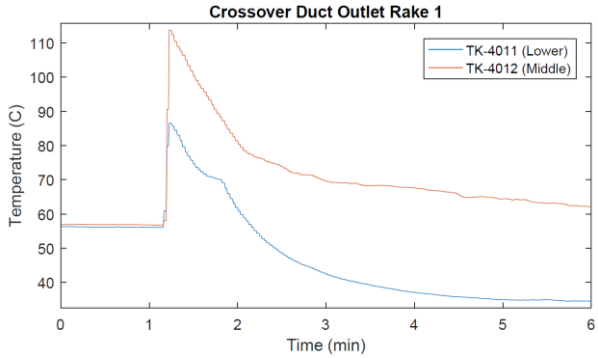

Figure 47: DCC 4 rake 1 temperatures in the hot leg.

To determine the time of slope and behavior change, the derivative the lower thermocouple from the cross-duct outlet rake one was taken, as shown below.

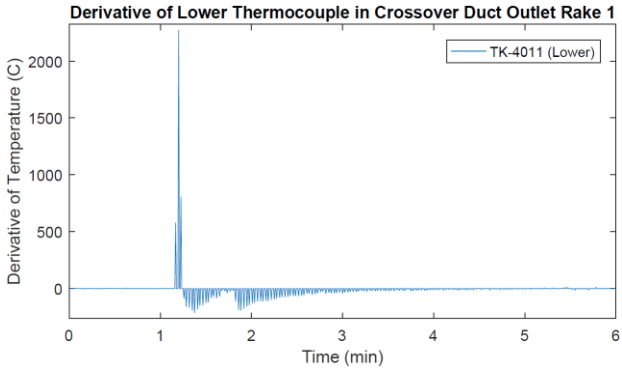

Figure 48: DCC 4 derivative of the lower thermocouple from Rake 1 in Figure 46.

The time of impact of the nitrogen layer with the bottom of the lower reflector was determined to be 110 seconds, using a threshold value of 10 times the noise value associated with the thermocouple; this is the value used in later results exploring lower plenum lock exchange flow visualization. Noise can be deduced from the derivative plots by examining slope change before the DCC event was started while the system was at steady state. 110 seconds is suspected to be the time when the lower plenum is filled up to the bottom of the lower reflector core block, which would significantly decrease the amount of helium moving out through the duct. The channels at the bottom of the lower reflector would be mostly blocked by the growing nitrogen layer. The middle thermocouple also changes its behavior a few seconds later indicating a change in heat transfer and interphase mixing.

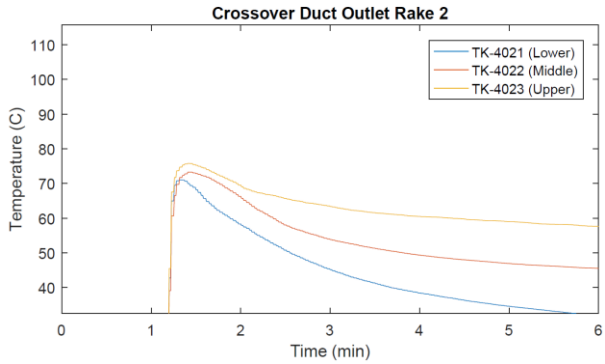

Figure 49: DCC 4 rake 2 measurements of the hot leg near RCST

Rake two in Figure 49 in the hot leg also shows the stratified flow behavior of lock exchange flow. The upper region would be helium flowing into the RCST, the middle showing mixing and interphase behavior and the lower thermocouple measuring the temperature of the nitrogen coming from the RCST. The upper thermocouple in rake two also has a slight change of behavior at around 120 seconds,

which is around the same time that there are indications of a full plenum up to the gas inlet level, as shown in Figure 50.

When comparing rake 1 in the hot leg Figure 47 and rake 2, clear changes in temperature are observed. The middle thermocouple in rake 1 ends at 6 minutes around 62ºC, while the middle thermocouple in rake 2 ends at around 45ºC.

Derivatives were also taken of the temperature profiles for the lower plenum posts. The momentum flow after the depressurization obscured the initial interactions of the nitrogen gas front in the lower plenum. Therefore, instead of looking for the first interaction, the last interaction was explored. The last significant interaction at the 75% level in the lower plenum is seen in Figure 50 below. Many of the values are around 110 seconds, which is the same time that it is postulated that the nitrogen gas layer made contact with the lower reflector block, which reduced the gas flow rate of helium out through the crossover duct. The color bar is representative of time in seconds.

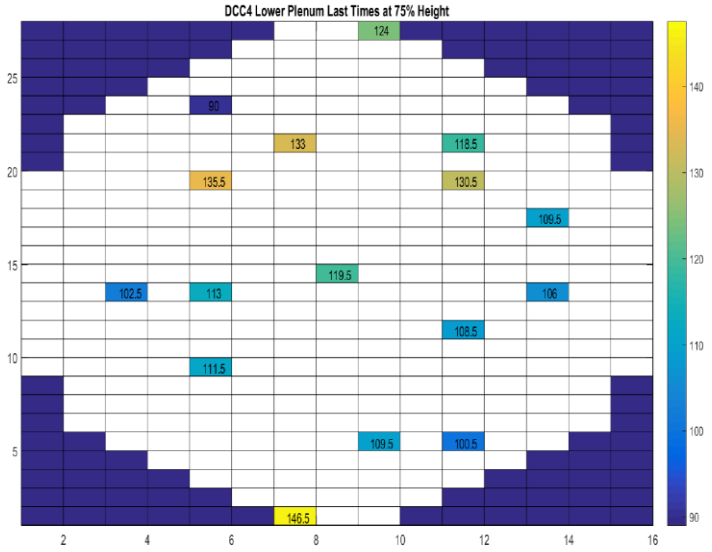

Figure 50: DCC 4 time indication of gas front moving through the lower plenum posts at 75% height.

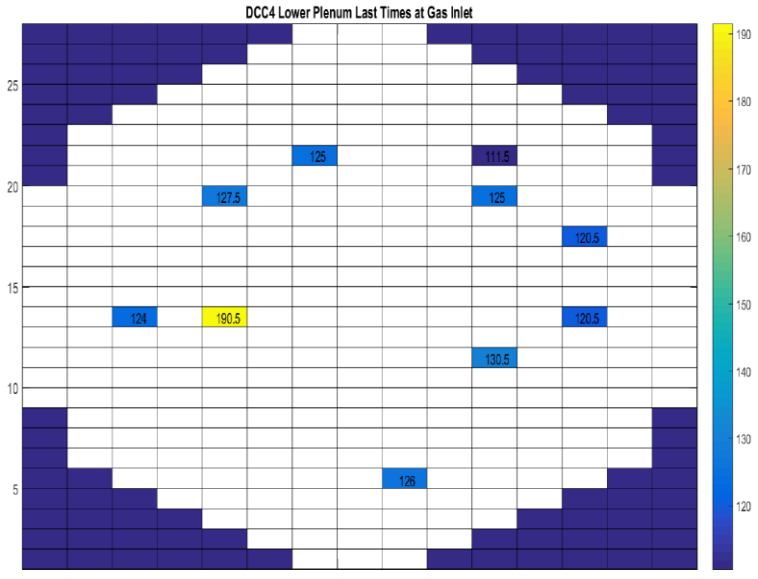

Figure 51: DCC 4 time indication plot of the Gas Inlet thermocouples for DCC 4.

In the gas inlet time plot, the time around 120 seconds, is around the same time that there was indication of a behavior shift in the helium flow in the hot leg rake two. Overall, the time of the last major temperature change measured in the gas inlet thermocouples are mostly similar.

The graphs and derivatives of the plenum posts show behavior shifts around 110 and 120 seconds, as the nitrogen gas front reaches the top of the lower plenum roof, restricting helium flow out of the vessel into the duct, lessening the amount of heat in the lower plenum creating a cooling effect on the thermocouples. The impact on the lower plenum roof core block propagates through the hot leg as well, with response at 110 seconds. Many of the lower plenum posts also displayed a shift in behavior around 110 seconds as shown in Figure 52. A reduced outflow of helium, reduces the amount of turbulent heat exchange that can occur between the two gas layers in the cross over duct, reducing the temperature at the thermocouples. The nitrogen will continue to intrude until the top elevation of the hot duct is met. The nitrogen layer fills up from the upper thermocouples on the posts to the gas inlet where the thermocouples are placed at the top of the post in the middle of the coolant channels in about 10 to 15 seconds, when comparing Figures 50 and 51.

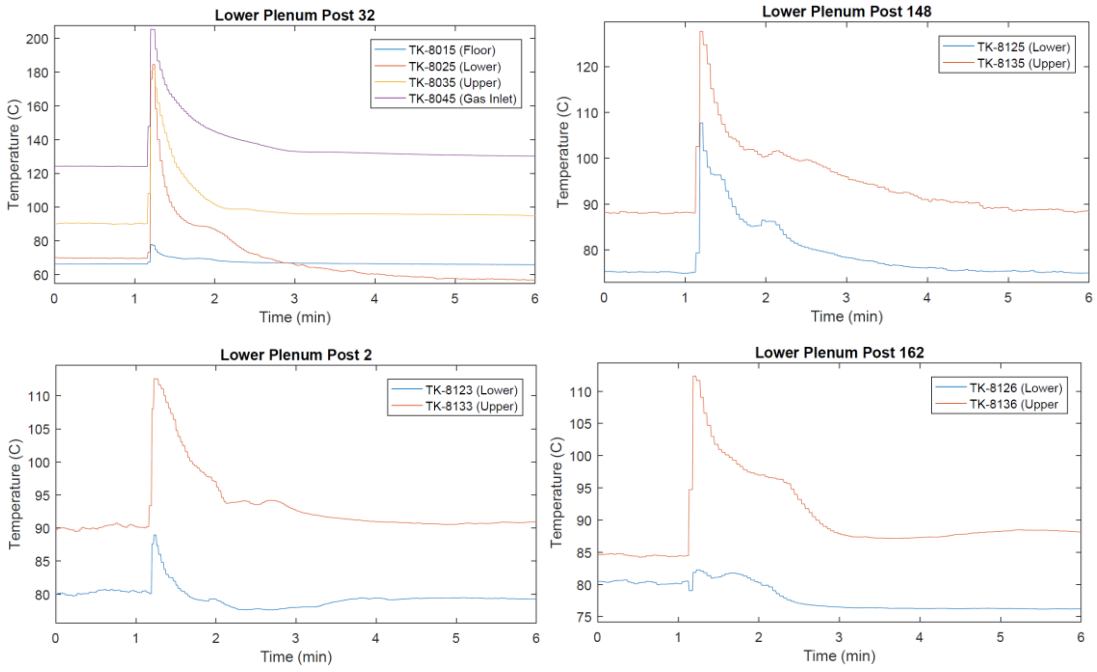

Figure 52: The figures above show posts 148, 32, 2, and 162.

4.2.1 Lower Plenum Results

Next the results in the lower plenum are shown. The post temperatures are recorded at a certain height, mapped, and interpolated between the temperatures using a linear least squares model from the inpaint_nans code [46]. The outer edges are extrapolated so they are not colored.

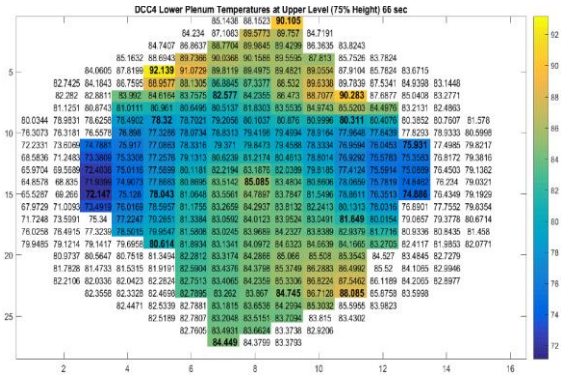

Figure 53: Shows the lower plenum temperatures and interpolation for DCC 4 before the accident at the upper thermocouple level.

Figure 53 above shows the steady state condition of the lower plenum before the experiment was initiated, but when the depressurization occurred, hot gas was pushed down by gas expansion through the coolant channels to the lower plenum shown in the subsequent seconds with the image compilation on the next page.

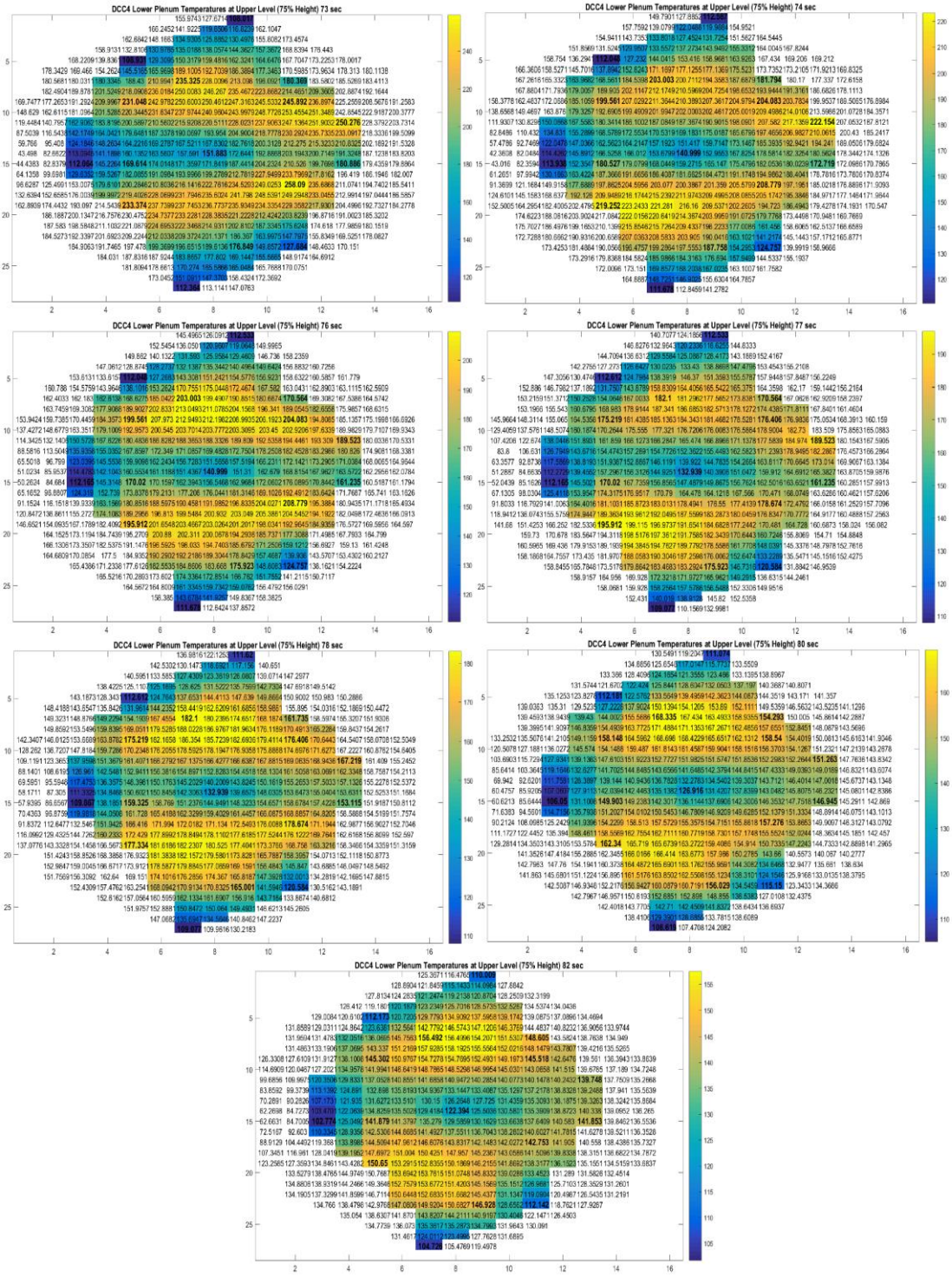

Figure 54: Shows the lower plenum temperatures and interpolation for DCC 4 during the depressurization and momentum flow caused by depressurization.

Figure 54 shows the same level of thermocouples at the 75% height, but in the subsequent seconds. The depressurization pattern is related to the flow channels in

the core. There are no flow channels in the center, and from there the flow channels bloom outwards. This pattern potentially obscures some lock exchange flow phenomena, as the gas front could be entering the lower plenum during these earlier seconds. However, the ensuing expansion of gas and momentum driven flow after the depressurization clearly changes the temperature profile of the lower plenum and the starting conditions of lock exchange flow. Therefore, finding phenomena related to lock exchange flow was be focused after 110 seconds, where phenomena was seen in rake one and the lower plenum upper thermocouples indicating a clear nitrogen interaction. The pre-test calculations suggest from Utberg that lock exchange flow will be finished and a quasi-equilibrium state achieved in less than 40 seconds for the most similar density gradient simulation case, but it does not consider any depressurization [9]. Additionally, in the simulation it was not considered that the lower plenum roof steps down into the area where the lower plenum would be, which could extend fill times by adding more hydraulic resistance. The gas inlet times show significant temperature change until around 120 seconds, which is thought to be when the lower plenum is full up to the top elevation of the hot duct.

4.3 DCC 5

DCC 5 is the only heated test to open both the cold and the hot leg valves. The test was conducted at equal pressures with a large density gradient. The lower plenum was much hotter than the RCST, as shown in comparing Figures 55 and 56 below. DCC 4 also had a large thermal difference, however the depressurization could have obscured a lot of relevant phenomena.

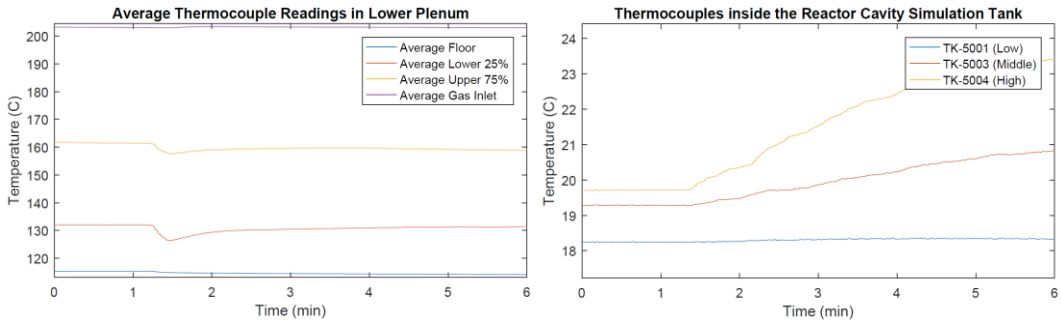

Figure 55: DCC 5 average lower plenum temperatures at each height
Figure 56: The RCST temperatures for DCC 5

The RCST temperatures steadily rise and stratify. The lower thermocouple changes very little. The hot helium immediately travels to the top of the RCST. The RCST has a much larger volume than the PPV, so the rise in overall RCST temperature is slight.

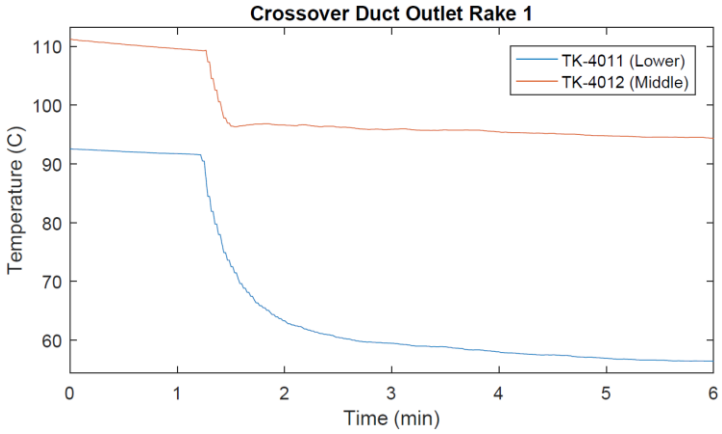

Figure 57: DCC 5 rake one in the hot leg near the PPV.

Figure 57 showing rake one is first measuring the helium inside the pipe. It is already stratified in the pipe with temperatures of helium. Then the nitrogen gas front propagates along the bottom of the pipe past rake one. It decreases the temperature of the lower thermocouple. The middle thermocouple measures the nitrogen gas front as well because the nitrogen layer should be larger than half of the hot leg pipe but has a larger heat transfer and mixing interphase influence from the hot helium atop the nitrogen. The thermal mixing between the two layers is consistent as shown with the slight slope of the line, however, it does slowly decrease suggesting that there is more nitrogen in the pipe than helium as time passes.

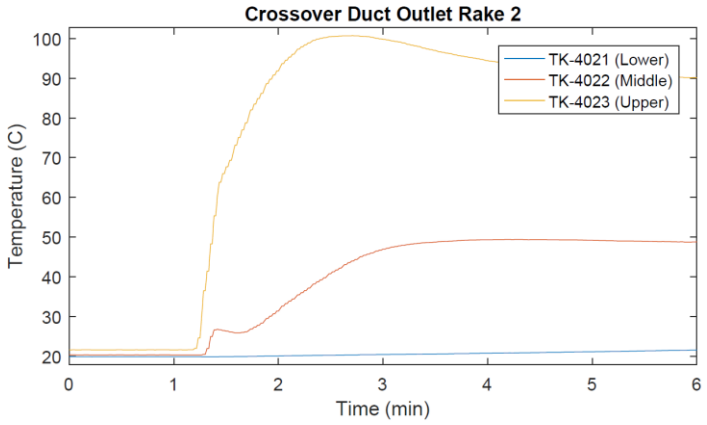

Figure 58: DCC 5 rake 2 in the hot leg near the RCST.

Figure 58 with rake two shows that the helium front first impacts the upper thermocouple. The helium displaces nitrogen that was stratified at the top of the pipe. This nitrogen from the top of the pipe is pushed downwards into the middle thermocouple. It is speculated that in response to the displaced nitrogen stratified at the top of the pipe, the middle thermocouple increases in temperature. Afterwards it is suspected that it measures rake interference and then the interphase and thermal transfer between the two layers of gas. Around 2 and a half minutes the amount of helium passing through the top of the pipe decreases as shown by a change in slope. This decrease suggests that the nitrogen gas has met the top of the lower plenum roof. This creates a bubble of helium and the nitrogen continues to rise slowly though the lower roof block to the quasi-equilibrium point of two thermally stratified gas layers.

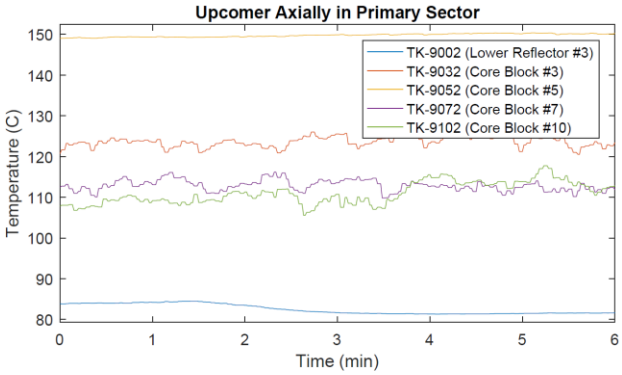

Figure 59: The upcomer temperature profile for DCC 5

The upcomer profile in Figure 59 shows that the middle of the core is the hottest, and that it is stratified.

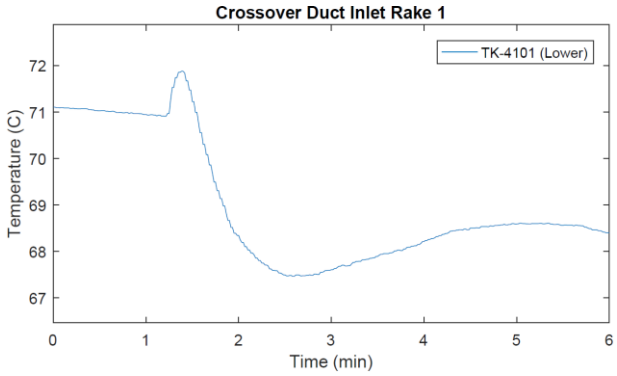

Figure 60: DCC 5 rake 1 in the cold leg near the PPV.

The helium flows out of the upcomer shown in Figure 60, raising the temperature of the thermocouple, but the concentric nature of the pipe allows

entrance to the outlet from various un-instrumented directions. In addition to being concentric at the inlet to the lower plenum, the cold leg is funneled and makes a 90 degree turn into a separated pipe, as displayed in the drawings in the Materials and Methods section. Then the singular pipe turns again to continue towards the cold leg break valve and the RCST. These features complicate the flow inside the pipe as seen by the thermocouples in the rakes. Thus, the increase in temperature is most likely the nitrogen gas front creating mixing and turbulence to displace hot helium and then decreasing the temperature as the nitrogen fills the bottom of the shell of the cold leg pipe in a more stabilized fashion.

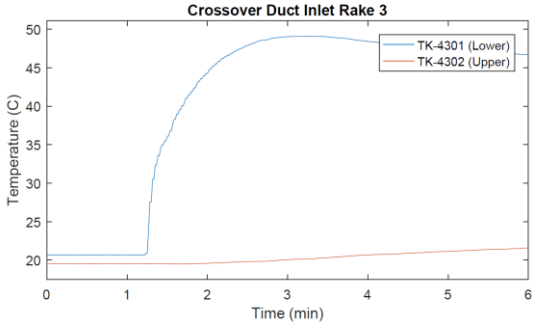

Figure 61: DCC 5 rake 3 in the cold leg near the RCST.

Figure 62 with rake three from the cold leg has an increasing lower thermocouple, however, it would have been hypothesized that helium would be flowing at the top of the pipe, raising the temperature of the upper thermocouple. Instead, the upper thermocouple increases gradually and the lower thermocouple, which would be expected to observe the nitrogen, increases. This behavior is thought to be residual of the geometry of the pipe between the PPV and the RCST even though rake three is in the separated part of the pipe close to the RCST where lock exchange flow would have been more stabilized.

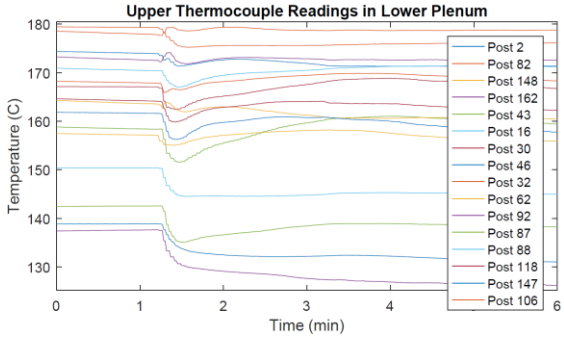

Figure 62: Shows all the upper thermocouple measurements in the posts in the lower plenum.

Figure 62 is only to show that all the thermocouples respond at roughly the same time at the same height of measurement and that there are a few outliers that increase in temperature instead of decrease. The increasing thermocouples are shown in the Figure 63 below.

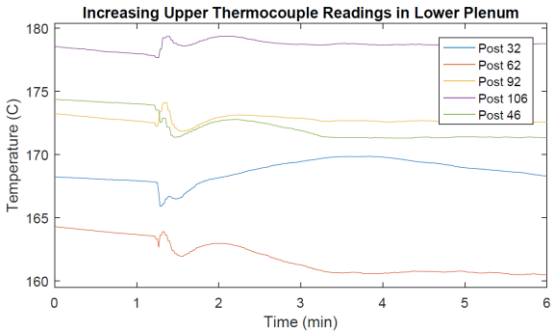

Figure 63: The upper thermocouples in the lower plenum posts that have initial increases in temperature.

The lower plenum posts that increase in temperature initially are closest to the outlet pipe. This is because the nitrogen gas enters the lower plenum, which is measured by the level of lower thermocouples in the posts, and displaces the hot helium upwards into the upper thermocouples. This is confirmed in the subsequent plot showing that most of these thermocouples significantly decrease at the lower level at the same time, expect for post 46 which is suspected to be experiencing a large amount of turbulence due to positioning in-between the edge of the core and the middle of the core. As seen in Figure 10 from the literature review section, the posts between the middle and the edge are enveloped last [35]. The edge represents the path of least flow resistance and the middle of the plenum is where inertia will carry the flow coming out of the outlet pipe. The posts between the middle and the edge, therefore, see the most disturbed gas front and the most mixed fluid from vortices created behind the cylinders [33].

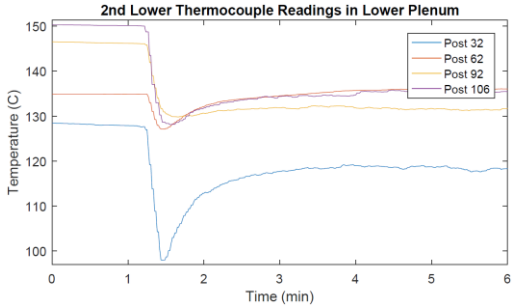

Figure 64: These posts are the closest to the hot duct outlet and thus generally see the largest changes from the nitrogen gas front.

Post 32, 62, 92 and 106 shown in Figure 64 had increasing upper thermocouple readings in the posts because of the arrival of the nitrogen gas front on the lower level. Post 46 also increased in the upper, however, it increased in the lower as well and it shows signs of turbulence in wavy and uncertain behavior in the plot of upper thermocouple readings as well as the temperature plot of lower thermocouple readings shown later. As described in the literature review, the low and Froude high Reynolds numbers will influence the shear stress at the boundary and create more interphase mixing. The cylinders will also introduce wake and mixing. It is also possible that the increase in temperature and the behavior of the post thermocouples are a function of the post orientation. If post 46 thermocouples are pointed towards the outlet pipe, they may see more gas front phenomena, if they are pointed away, they may see more wake mixing phenomena, which may explain why some mirrored posts see different behavior.

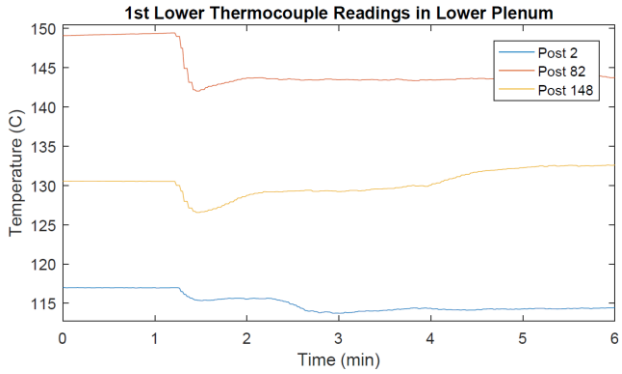

Figure 65: Shows addition lower thermocouple readings of posts that have decreasing temperature trends during DCC 5.

With Figure 65 shown above, post 2 is on the very edge of the core to the north of the center. As an alcove, it may experience little direct contact with the gas front or observe the gas front as it bounces of the walls nearby. Post 148 is on the southern edge of the core closer to the outlet duct, therefore it sees a large temperature change as the gas front arrives and circumnavigates the center of the core to avoid large form loss in the posts. Post 82 is in the very center of the core and it sees the nitrogen gas front a few seconds after post 148, because travelling through the center of the core takes a longer time. The gas front impact on the thermocouple

is also less significant because it has been lessened by form loss, mixing, and heat exchange with the helium.

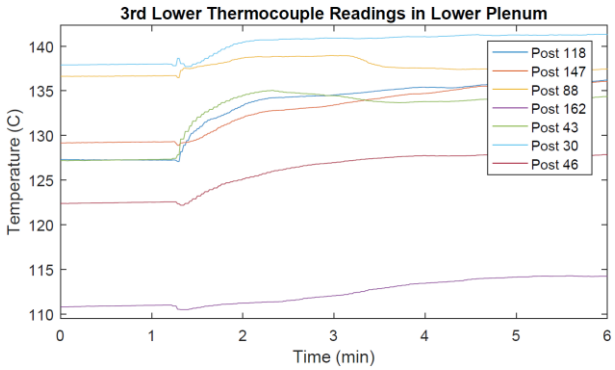

Figure 66: Lower thermocouple post readings for DCC 5 with increasing temperature trends.

In Figure 66, posts 43 and 118 have the largest increasing trend. They mirror each other in the back of the lower plenum north and south of the center. Post 88 is thought to experience the most turbulence, along with 118 and 43 because of their placement in the back of the plenum. Other studies have found that the gas front will bounce off of the back plenum wall, which could create unstable conditions in the back [15], [16]. Post 46 is close to the edge and is only one post away from post 32, which has a large initial decreasing trend. It is suspected that post 46 is responding to this shift in post 32; as the gas front interacts with post 32, the displaced gas must move away and thus it is suspected it moves toward post 46. As the nitrogen gas front travels around the edge of the core, the heated helium is displaced to other areas of the core. Posts 147 and 30 also see similar phenomena as post 46, in that posts 30, 46, and 147 are close to the edge of the core, however, the gas front skirts the posts, which moves the warm displaced helium into those posts. Post 162 is on the very edge of the core to the south of the center. As an alcove, it experiences local mixing and turbulence with little direct contact with the gas front.

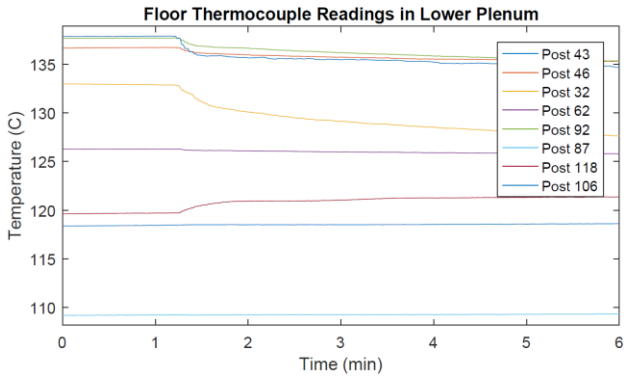

Figure 67: DCC 5 floor thermocouple readings on the posts.

In Figure 67, all the floor thermocouples in the posts decrease in temperature except for in post 118, where there is the most turbulent mixing in the core. This turbulent mixing phenomena is confirmed in images to follow of the lower plenum visualization as well as the timing of the nitrogen gas front. The hot spot in the core was moved back to around post 118 as lock exchange flow occurred.

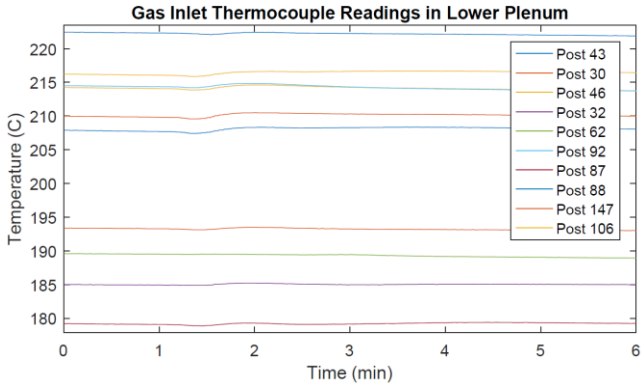

Figure 68: DCC 5 gas inlet readings on the posts.

As shown in Figures 67 and 68, the floor and the gas inlet thermocouples have a smaller response to the gas front from the RCST because they are closer the core blocks which have a high thermal mass. Gas inlet phenomena was obscured in DCC 5 while visible in DCC 4 because the core was not uniformly heated in DCC 4. The mixing and heat transfer in DCC 4 was less important and thus the gas inlet thermocouples showed significant phenomena. The gas inlets in DCC 5 show a small dip and a small increase in temperature as the nitrogen enters and helium exits, but are overall less indicative as gas inlets than DCC 4.

4.3.1 Lower Plenum Results

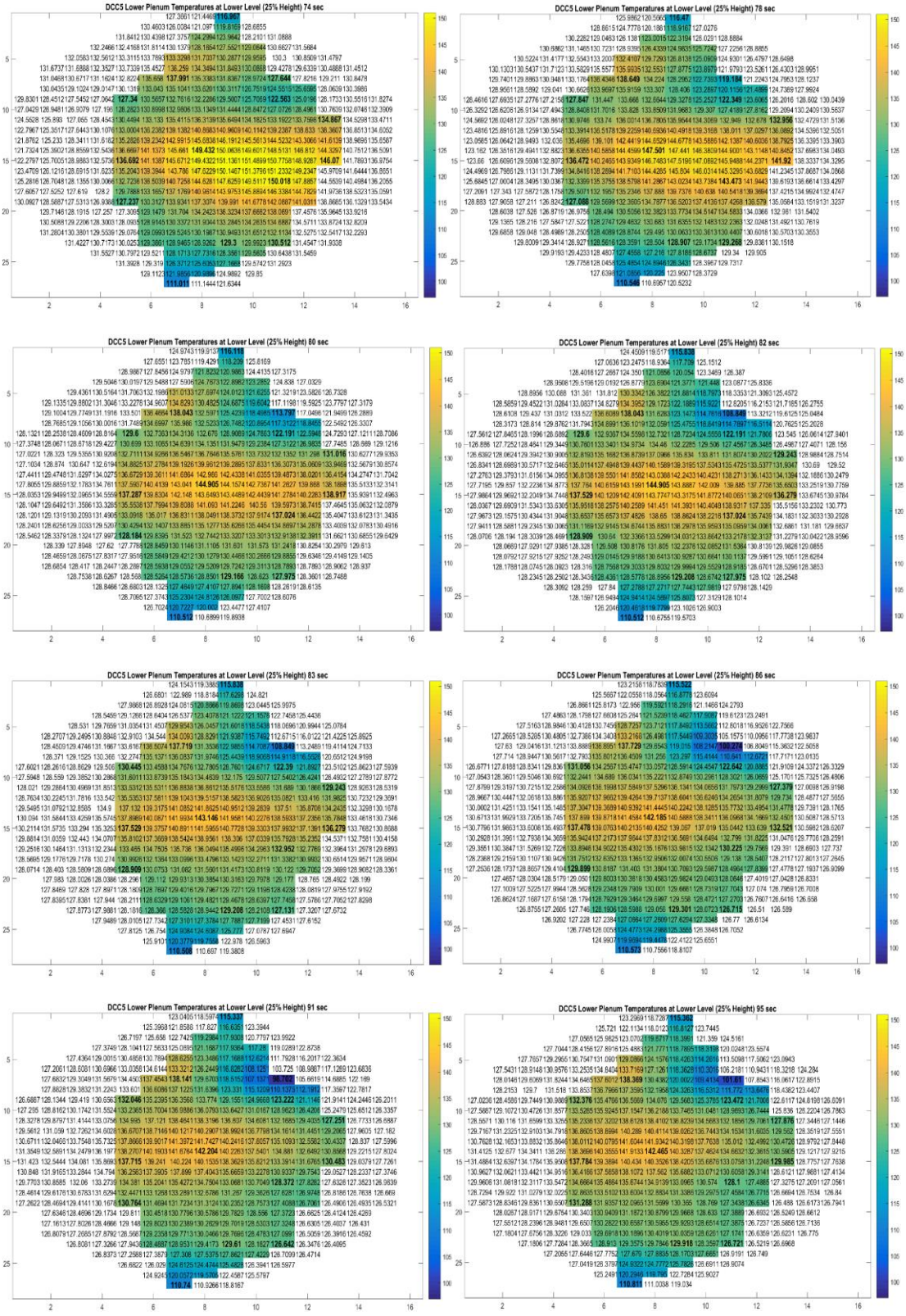

Figure 69: Shows the behavior of the lower plenum at the lower thermocouple level (25%) during lock exchange flow with the scale between 97 and 151ºC. The outlet pipe is on the right.

In the collection of images in Figure 69, the nitrogen enters the lower plenum on the right side and can be seen travelling around the sides of the lower plenum, it is especially visible as it moves the hot spot of the lower plenum back. It is suspected there is turbulence in the back of the plenum which circulates and could have bounced back off the back wall of the lower plenum. The behavior of the back of the plenum can be further seen when interpreting the times at which the gas front arrives at each post, displayed below.

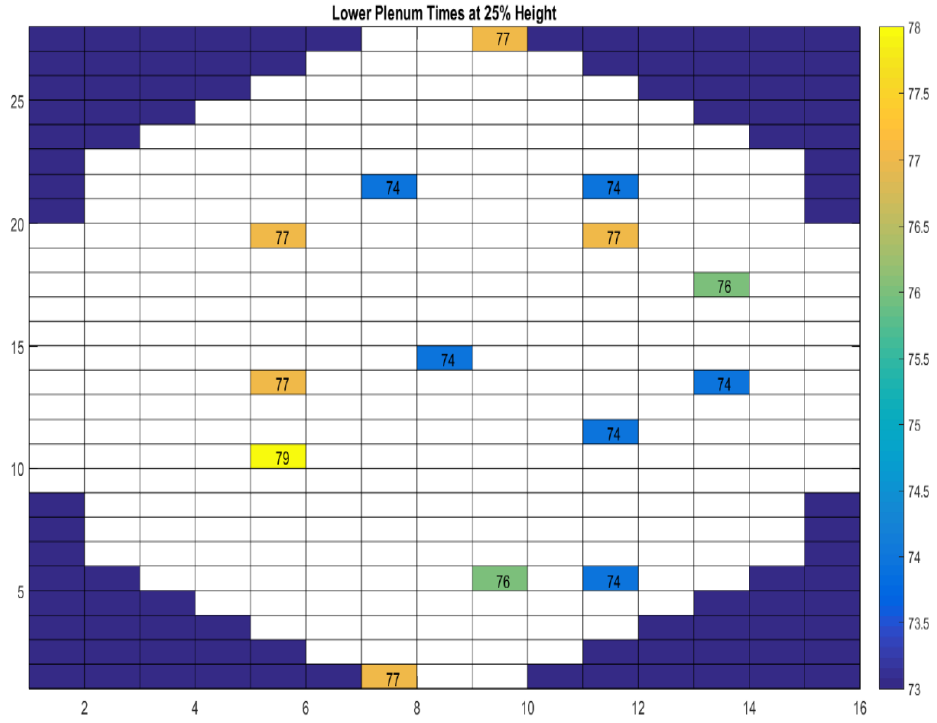

Figure 70: Shows the time when the nitrogen gas front interacts with the lower thermocouple in each working post.

The times are the smallest around the entrance of the lower plenum and the edges. The very edge of the lower plenum is insulated from change as the cold front bypasses the alcoves. The middle of the core tends to take a longer time to see the nitrogen gas front because it must travel between posts and experiences form losses and slows in the plenum. The back thermocouples observe the nitrogen front last as the front dematerializes and becomes turbulent mixing of the nitrogen and the helium and the gas front rebounds off the back wall of the plenum.

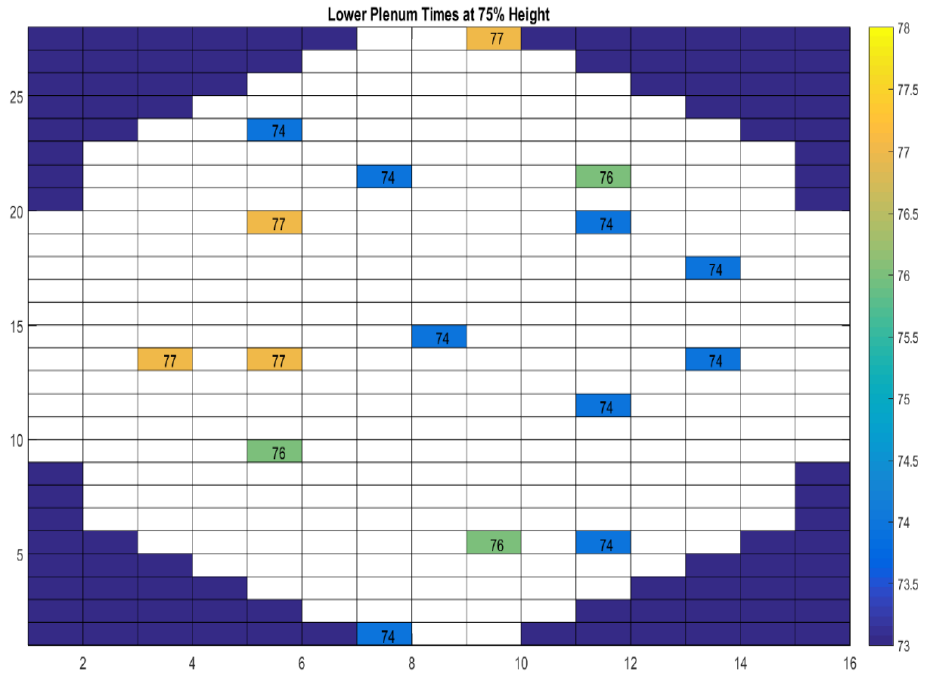

Figure 71: Measurement of first time of impact in the upper thermocouples of the posts.

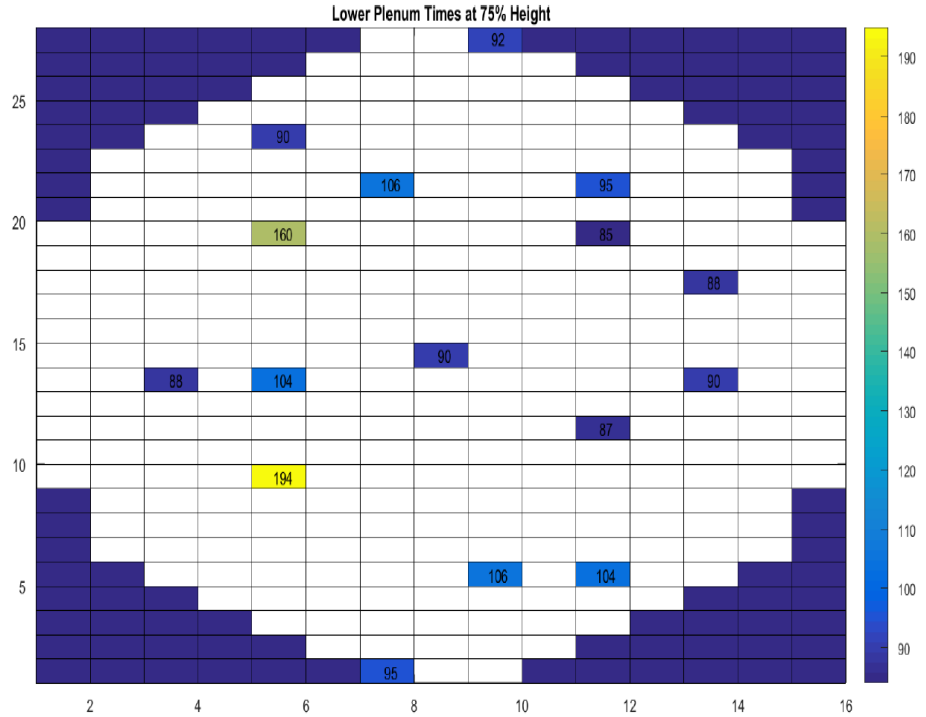

Figure 72: Measurement of the last time of significant temperature change in the upper thermocouples of the posts.

Entrance behavior of the nitrogen gas front is observed in both images above depicting the times of significant change in the temperatures of the upper

thermocouple instrumentation in each of the posts. In the first image, the gas front enters the core and flows through the center and around the edges, meeting at the back of the lower plenum at about the same time. The second image shows that the last time the temperature changes significantly also moves in the gas front pattern; the entrance sees change, with that change blooming outwards and with high amounts turbulence and rebound in the back of the plenum.

5. Discussion and Conclusions

5.1 Discussion

Various tests were able to address each of the time characteristics that were the objectives of this experiment. The first three ambient tests at equalized pressures could not clearly distinguish phenomena from the error of the instrumentation, although DCC 2 and DCC 3 were the only two tests repeated and thus the only observations that can be confirmed via repeatability. The heated tests were outside of instrument error therefore, they were studied more fully. Unfortunately, the time characteristics available for each of the heated tests, DCC 4 and DCC 5, were different so direct comparison for most cases is impossible.

5.1.1 Observance of Quasi-Equilibrium State

DCC 4 observed a quasi-equilibrium state for the onset of molecular diffusion around 125 seconds, roughly 1 minute after the hot leg valve was opened. It is speculated that DCC 2 and 3 achieved a quasi-equilibrium state around 3 and a half minutes after the initiation of the experiment. The isothermal tests took approximately two and a half more minutes to reach a quasi-equilibrium state than the heated test. The inlet rakes in the cold legs for DCC 2 and 3 also see subtle changes around 4 minutes.

5.1.2 Observance of Lower Plenum Filling

Because DCC 4 was not uniformly heated like DCC 5, the lower reflector core block and the floor was at a lower temperature than the middle of the core. When the nitrogen gas entered, it experienced less heat transfer from the core blocks and less mixing with more uniformly heated helium. Less heat transfer allowed the gas inlet thermocouples to observe a significant change in temperature when the nitrogen travelled up the lower plenum reflector block to the height of the gas inlet thermocouples. The difference between the time of impact in the upper thermocouples in DCC 4 and the gas inlet thermocouples could then be calculated to be about 10 to 15 seconds.

DCC 4 indicated that the upper thermocouple level was achieved around 110 seconds seen in Figure 50, this is also suspected to be when the gas front interacts

with the lowest lower reflector core block that intrudes down into the lower plenum by observation of rake one in the hot leg. Impinging on the lower reflector core block would significantly lower the amount of helium moving out of the pressure vessel. It creates a helium "bubble" above that has still not reached equilibrium because the nitrogen has not reached the highest elevation of the hot duct. During DCC 4, the gas inlet thermocouples have their last large thermal response around 120 to 125 seconds as seen in Figure 51, indicating that the volume between the upper thermocouples in the posts and the gas inlet thermocouples took 10 to 15 seconds to fill. The onset of natural circulation is speculated to be between 120 and 125 seconds, when the lower plenum is filled up to the top of the gas inlet thermocouples.

5.1.3 Observance of Gas Front Arrival at the Lower Plenum Posts

DCC 5 did have some distinct advantages to DCC 4. As the pressure vessel depressurized, the gas in the vessel expanded. The cold leg was not opened, so gas in the cold leg expanded and pushed gas up the upcomer into the upper plenum, the gas was then forced down through the core. The hot gas arrived at the lower plenum creating a distinct coolant channel pattern. The momentum of the depressurization flow obscures the decrease in temperature in the lower level of thermocouples in the lower plenum which could have been introduced by a nitrogen gas front. In DCC 5, the arrival of the nitrogen gas front at each one of the instrumented lower plenum posts is clear on the lower level of thermocouples in the posts. There is a significant temperature change above the error threshold between 74 and 77 seconds for all of the instrumented posts that display a blooming pattern from the entrance of the hot leg.

In DCC 5, mixing and turbulence in the lower plenum is speculated with the movement of temperatures from the middle of the core towards the back. Studies have hypothesized that the gravity current bounces off the back wall of the lower plenum, creating mixed conditions. The areas in-between the edges and the middle experience turbulence and mixing as the nitrogen gas eventually envelops them, but experiences the most loss in doing so. It takes a longer time to reach these locations and causes temperature fluctuations in the thermocouples in those posts between the edge of the plenum and the middle.

5.1.4 Speed of the Gas Front

DCC 5 lower plenum thermocouples responded at 74 seconds, the same time that the rake thermocouples in the hot leg respond to nitrogen gas front, suggesting that the average speed of the gas front is at least .95 m/s. Speeds were difficult to determine with the 1 Hz data acquisition.

5.2 Future Work

Oh found that it can be assumed that the lock exchange flow phenomena can be assumed to be an instantaneous process thus the final air distributions are more important than the detail transitions of the phenomenon [40]. As the temperature of the core increases, the nitrogen in the HTTF will be heated and expand upwards into the core. The remaining helium will be pushed up and out of the core. The expansion effect diminishes with temperature because the specific volume is inversely proportional to the core temperature by the ideal gas law so the higher temperature expansion is very slight, as can be seen in the figure below [23], [40]. In addition, the heat up of the air inside the lower plenum will contribute further to its buoyancy inside the reactor to accelerate the onset of natural circulation [22].

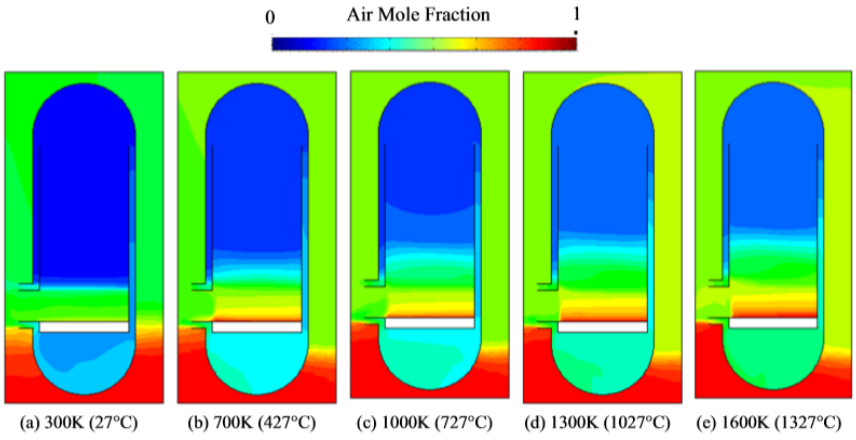

Figure 73: Air level in core after 90 seconds [40][12]

The HTTF has Gas Concentration Instruments (GCIs) that were developed at Oregon State University [47], which would be able to record the concentration of nitrogen and helium at each GCI location in the rakes, lower plenum posts, and

[12] "Reprinted from Experimental Validation of Stratified Flow Phenomena, Graphite Oxidation, and Mitigation Strategies of Air Ingress Accidents INL/EXT-08-14840, Chang H. Oh, Eung S. Kim, Hee C. NO, and Nam Z. Cho, page 2-27, December 2008, with permission from INL."

RCST, but the GCIs were not working for these experiments. Nitrogen expansion is not measurable with thermocouples after the nitrogen is heated and mixes with the helium; thus, to observe this process further work should be done to ensure the use of the GCIs.

The lower plenum posts and the rakes measured the nitrogen gas front at the same time and thus it was not possible to measure the exact speed of the front moving in the duct, but only the minimum speed. The time frame was too short to realistically measure with instrumentation taking one measurement per second. With a higher measurement rate, the speed of the front depending of density difference between the cavity and the pressure vessel could be studied.

More tests should be conducted with various density gradients and Reynolds numbers to create a parametric study of the factors that change lock exchange flow. More tests will allow for more confidence in postulations. Tests at full operating temperatures should be repeated for confirmation of results.

6. Bibliography

[1] R. Schultz *et al.*, "Next Generation Nuclear Plant Methods Technical Program Plan," Idaho National Laboratory, Department of Energy Office of Nuclear Energy INL/EXT-06-11804, Jan. 2007.

[2] M. Tonogouchi *et al.*, "Plant Concept of Heat Utilization of High Temperature Gas-Cooled Reactors," presented at the JAERI Conference 96-010.

[3] A. Shenoy *et al.*, "Gas Turbine-Modular Helium Reactor (GT-MHR) Conceptual Design Description Report," General Atomics, 910720, Jul. 1996.

[4] C. Oh, E. Kim, H. Kang, H. No, and N. Cho, "FY-09 Report: Experimental Validation of Stratified Flow Phenomena, Graphite Oxidation, and Mitigation Strategies of Air Ingress Accidents," Idaho National Laboratory, Department of Energy Office of Nuclear Energy INL/EXT-09-16465, Dec. 2009.

[5] C. Oh and E. Kim, "Isothermal Air-Ingress Validation Experiments," *Nucl. Technol.*, vol. 181, pp. 68–80, Jan. 2013.

[6] J. Kim, J.-S. Hwang, E. Kim, B. Kim, and C. Oh, "Experimental study on fundamental phenomena in HTGR small break air-ingress accident," *Ann. Nucl. Energy*, Aug. 2015.

[7] A. J. Neylan and W. Simon, "Status of the GT-MHR," presented at the JAERI Conference 96-010, pp. 89–96.

[8] K. Kugeler, "Nuclear Safety and the Expectation to HTGR's Deployment," presented at the JAERI Conference 96-010, pp. 21–35.

[9] J. Utberg Jr, "Nitrogen Concentration Sensitivity Study of the Lock Exchange Flow Phenomenon in the High Temperature Test Facility," 2013.

[10] S. Ball, M. Richards, and S. Shepelev, "Sensitivity studies of air ingress accidents in modular HTGRs," *Nucl. Eng. Des.*, vol. 238, pp. 2935–2942, 2008.

[11] C. Oh and E. Kim, "Air-Ingress Analysis: Part 1. Theoretical Approach," *Nucl. Eng. Des.*, vol. 241, pp. 203–212, 2011.

[12] B. Woods, R. Jackson, B. Nelson, and S. Cadell, "Scaling Analysis for the Very High Temperature Reactor Test Facility at Oregon State University." .

[13] R. Jackson, B. Woods, J. Utberg Jr, and S. Cadell, "Instrumentation Plan for the High Temperature Test Facility at Oregon State Unversity." .

[14] J. Magnusson, "Pressure Effects on Density-Difference Driven Stratified Flow: CFD Model of a DCC event in the HTGR," 2011.

[15] I. Gutowska, "Study on Depressurized Loss of Coolant Accident and its Mitigation Method Framework at Very High Temperature Gas Cooled Reactor," 2015.

[16] D. Arcilesi Jr., T. Ham, I. Kim, X. Sun, R. Chirstensen, and C. Oh, "Scaling and design analyses of a scaled-down, high-temperature test facility for experimental investigation of the initial stages of a VHTR air-ingress accident," *Nucl. Eng. Des.*, vol. 288, pp. 141–162, Mar. 2015.

[17] A. Kadak and T. Zhai, "Air Ingress Benchmarking with Computational Fluid Dynamics Analysis," *Nucl. Eng. Des. Elsevier*, no. 236, pp. 587–602, 2006.

[18] T. Takeda, M. Hishida, S. Imanishi, and S. Takenaka, "Analysis of Air Ingress Process During the Primary-Pipe Rupture Accident of the HTGR," presented at the JAERI-Conf 96-010, 1996, pp. 272–288.

[19] S. Ball and S. Fisher, "Next Generation Nuclear Plant Phenomena Identification and Ranking Tables (PIRTs)," Oak Ridge National Laboratory, United States Nuclear Regulatory Commission NUREG/CR-6944 Volume 1, Mar. 2008.

[20] J. Graves, "Top-Down Scaling Analysis of the Integral Reactor Vessel Test Facility," Oregon State University, 2012.

[21] T. Ham *et al.*, "Computational fluid dynamics analysis of the initial stages of a VHTR air-ingress accident using a scaled-down model," *Nucl. Eng. Des.*, vol. 300, pp. 517–529, 2016.

[22] C. Oh, E. Kim, H. No, and N. Cho, "Final Report on Experimental Validation of Stratified Flow Phenomena, Graphite Oxidation, and Mitigation Strategies of Air Ingress Accidents," Idaho National Laboratory, INL/EXT-10-20759, Jan. 2011.

[23] C. Oh, E. Kim, R. Schultz, D. Petti, and C. Liou, "Implications of Air Ingress Induced by Density-Difference Driven Stratified Flow," presented at the ICAPP 2008, Anaheim, California, 2008.

[24] T. Benjamin, "Gravity currents and related phenomena," *J. Fluid Mech.*, vol. 31, no. 2, pp. 209–248, 1968.

[25] C. Liou, R. Schultz, and Y. Kukita, “Stably Stratified Flows in Closed Conduits,” presented at the 5th International Conference on Nuclear Engineering (ICONE5), Nice, France, 1997, pp. 2–24.

[26] J. S. Turner, *Buoyancy Effects in Fluids*. 1973.

[27] R. Lowe, J. Rottman, and P. Linden, “The non-Boussinesq lock-exchange Problem. Part 1. Theory and Experiments,” *J Fluid Mech*, vol. 537, pp. 101–124, 2005.

[28] V. Birman, J. Martin, and E. Meiburg, “The non-Boussinesq lock-exchange Problem. Part 2. High-Resolution Simulations,” *J Fluid Mech*, vol. 537, pp. 125–144, 2005.

[29] R. Lowe, P. Linden, and J. Rottman, “A laboratory study of the velocity structure in an intrusive gravity current,” *J. Fluid Mech.*, vol. 456, pp. 33–48, 2002.

[30] Y. Hassan, “Study of Air Ingress Across the Duct During the Accident Conditions,” Texas A&M University, Project No. 09-841, Oct. 2013.

[31] J. Hacker, P. Linden, and S. Dalziel, “Mixing in lock-release gravity currents,” *Dyn. Atmospheres Oceans*, vol. 24, pp. 183–195, 1996.

[32] A. Wirth, “Mixing in Stratified Shear Flow,” in *A Guided Tour Through Buoyancy Driven Flows and Mixing*, 2014.

[33] J. Holford and P. Linden, “Turbulent mixing in a stratified fluid,” *Dyn. Atmospheres Oceans*, vol. 30, pp. 173–198, 1999.

[34] C. Staquet and J. Sommeria, “Internal waves, turbulence and mixing in stratified flows: a report on Euromech Colloquium 339,” *J. Fluid Mech.*, vol. 314, pp. 349–371, 1996.

[35] T. Ham, D. Arcilesi Jr., X. Sun, R. Chirstensen, C. Oh, and E. Kim, “Preliminary CFD Calculations for OSU Air-Ingress Experimental Facility,” in *Computational Thermal Hydraulics*, San Diego, California, 2012, vol. 107, pp. 1290–1292.

[36] C. Oh and E. Kim, “Air Ingress Analysis: Computational Fluid Dynamic Models,” presented at the International Heat Transfer Conference (IHTC14), Washington DC, 2010.

[37] C. Oh, E. Kim, R. Schultz, M. Patterson, D. Petti, and H. Kang, "Comprehensive thermal hydraulics research of the very high temperature gas cooled reactor," *Nucl. Eng. Des.*, vol. 240, pp. 3361–3371, Jul. 2010.

[38] C. Oh, E. Kim, R. Schultz, M. Patterson, and D. Petti, "Thermal Hydraulics of the Very High Temperature Gas Cooled Reactor," presented at the The 13th International Topical Meeting on Nuclear Thermal Hydraulics (NURETH-13), Kanazawa, Japan, 2009.

[39] C. Oh, H. Kang, and E. Kim, "Air-ingress analysis: Part 2. Computational fluid dynamic models," *Nucl. Eng. Des.*, vol. 241, pp. 213–225, May 2010.

[40] C. Oh, E. Kim, H. No, and N. Cho, "Experimental Validation of Stratified Flow Phenomena, Graphite Oxidation, and Mitigation Strategies of Air Ingress Accidents," Idaho National Laboratory, INL/EXT-08-14840, Dec. 2008.

[41] C. Oh and E. Kim, "Isothermal Air Ingress Validation Experiments at Idaho National Laboratory: Description and Summary of Data," Idaho National Laboratory, INL/EXT-10-19727, Sep. 2010.

[42] H. P. Grobelbauer, T. K. Fannelop, and R. E. Britter, "The propagation of intrusion fronts of high density ratios," *J. Fluid Mech.*, vol. 250, pp. 669–687, 1993.

[43] D. Lakehal and H. Lemonnier, "Test-Case No 28: The Lock-Exchange Flow," *Mutliphase Sci. Technol.*, vol. 16, no. 1–3, pp. 171–175, 2004.

[44] C. Oh and E. Kim, "Validations of CFD Code For Density-Gradient Driven Air Ingress Stratified Flow," presented at the 18th International Conference on Nuclear Engineering (ICONE18), Xi'an, China, 2010.

[45] S. Koehler, *Error Propagation*. MATLAB Central File Exchange: Mathworks, 2017.

[46] J. D'Errico, *inpaint_nans*. MATLAB Central File Exchange, 2017.

[47] S. Cadell, "Development of a Binary Mixture Gas Composition Instrument for Use in a Confined High Temperature Environment," 2012.

7. Appendices

Location	Instrument	Tag Number
4 TCs per post		
Post 43, gas inlet	Thermocouple	TK-8041
Post 43, upper	Thermocouple	TK-8031
Post 43, lower	Thermocouple	TK-8021
Post 43, floor	Thermocouple	TK-8011
Post 16, gas inlet	Thermocouple	TK-8042
Post 16, upper	Thermocouple	TK-8032
Post 16, lower	Thermocouple	TK-8022
Post 16, floor	Thermocouple	TK-8012
Post 30, gas inlet	Thermocouple	TK-8043
Post 30, upper	Thermocouple	TK-8033
Post 30, lower	Thermocouple	TK-8023
Post 30, floor	Thermocouple	TK-8013
Post 46, gas inlet	Thermocouple	TK-8044
Post 46, upper	Thermocouple	TK-8034
Post 46, lower	Thermocouple	TK-8024
Post 46, floor	Thermocouple	TK-8014
Post 32, gas inlet	Thermocouple	TK-8045
Post 32, upper	Thermocouple	TK-8035
Post 32, lower	Thermocouple	TK-8025
Post 32, floor	Thermocouple	TK-8015
Post 62, gas inlet	Thermocouple	TK-8046
Post 62, upper	Thermocouple	TK-8036
Post 62, lower	Thermocouple	TK-8026
Post 62, floor	Thermocouple	TK-8016
Post 92, gas inlet	Thermocouple	TK-8047
Post 92, upper	Thermocouple	TK-8037

Location	Instrument	Tag Number
Post 92, lower	Thermocouple	TK-8027
Post 92, floor	Thermocouple	TK-8017
Post 87, gas inlet	Thermocouple	TK-8048
Post 87, upper	Thermocouple	TK-8038
Post 87, lower	Thermocouple	TK-8028
Post 87, floor	Thermocouple	TK-8018
Post 88, gas inlet	Thermocouple	TK-8049
Post 88, upper	Thermocouple	TK-8039
Post 88, lower	Thermocouple	TK-8029
Post 88, floor	Thermocouple	TK-8019
Post 118, gas inlet	Thermocouple	TK-8140
Post 118, upper	Thermocouple	TK-8130
Post 118, lower	Thermocouple	TK-8120
Post 118, floor	Thermocouple	TK-8110
Post 147, gas inlet	Thermocouple	TK-8141
Post 147, upper	Thermocouple	TK-8131
Post 147, lower	Thermocouple	TK-8121
Post 147, floor	Thermocouple	TK-8111
Post 106, gas inlet	Thermocouple	TK-8142
Post 106, upper	Thermocouple	TK-8132
Post 106, lower	Thermocouple	TK-8122
Post 106, floor	Thermocouple	TK-8112
2 TCs per post		
Post 2, upper	Thermocouple	TK-8133
Post 2, lower	Thermocouple	TK-8123
Post 82, upper	Thermocouple	TK-8134
Post 82, lower	Thermocouple	TK-8124
Post 148, upper	Thermocouple	TK-8135

Location	Instrument	Tag Number
Post 148, lower	Thermocouple	TK-8125
Post 162, upper	Thermocouple	TK-8136
Post 162, lower	Thermocouple	TK-8126

Thermocouples that were not working due to cRIO failure during DCC 1 and DCC 2:

Post 87: TK8018, TK8028, TK8038, TK8048

Post 88: TK8019, TK8029. TK8039. TK8049

Post 118: TK8110, TK8120, TK8130, TK8140

Post 147: TK8111, TK8121, TK8131, TK8141

Other thermocouples that did not work during any of the experiments are:

Post 16: TK8012, TK8022, TK8042

Post 30: TK8013

Post 87: TK8028

Post 88: TK8019

Post 118: TK8140

Post 147: TK8111

Hot Leg Rake 1 (Close to PPV) Upper Thermocouple: TK4013

Cold Leg Rake 1 (Close to the PPV) Upper Thermocouple: TK4102